Copernicus Marine Service

QUALITY INFORMATION DOCUMENT

Near Real-Time IN SITU production centre

INSITU_GLO_PHY_UV_DISCRETE_NRT_013_048

Issue: 2.3

Contributors: Nathalie Verbrugge, Hélène Etienne, L. Corgnati, C. Mantovani, E. Reyes, L. Solabarrieta, A. Rubio, T Carval, Julien Mader, L. Drouineau

Approval date by the Copernicus Marine Service product quality coordination team: 18/12/2023

CHANGE RECORD

When the quality of the products changes, the QuID is updated and a row is added to this table. The third column specifies which sections or sub-sections have been updated. The fourth column should mention the version of the product to which the change applies.

Issue	Date	§	Description of Change	Author	Validated By
1.0	14/01/2019	All	Creation of the document	Nathalie Verbrugge, Hélène Etienne, Julien Mader, L. Corgnati, C. Mantovani, E. Reyes, A. Rubio	L. Petit de la Villéon
1.1	03/04/2019		Minor changes and approvement by the Product Quality group (Mercator-Ocean)		
2.0	29/11/2019	All	1st update of the document: Update of existing dataset (radar_total) Addition of a new dataset (radar_radial)	Lorenzo Corgnati, Carlo Mantovani, Emma Reyes, Anna Rubio, Julien Mader, Paz Rotllán, Nathalie Verbrugge, Hélène	
2.1	02/09/2020	All	Addition of Argo currents dataset	Thierry Carval	Stéphane Tarot
2.2	24/05/2022	All	New template, drifter_filt_removal, new data in MED, renaming of the product and datasets	N. Verbrugge, L. Drouineau, L. Corgnati, E Reyes	Stéphane Tarot
2.2	31/08/2022	§1.2.3 §2.3 §3.4	Update of Argo dataset figures	Thierry Carval	Stéphane Tarot
2.3	11/04/2023	I.2.1 II.1 I.2.3 II.3 IV.3	Add undrogued drifters. Update §V with mention of the decline in the number of drifters Update of figures and numbers	H.Etienne, N. Verbrugge, Thierry Carval	Stéphane Tarot

TABLE OF CONTENTS

GLOSSARY AND ABBREVIATIONS

Acronym	Description
Argo, Euro-Argo	International profiling float network (www.argo.net) and its European component (http://www.euro-argo.eu)
DBCP, ESURFMAR	Data Buoy collaboration panel (http://www.jcommops.org/dbcp/) and its European component (http://www.eumetnet.eu/e-surfmar)
SeaDataNet	European Network of National Oceanographic Data Centres (NODCs) (http://www.seadatanet.org/)
TAC	Copernicus Marine Service Thematic Assembly Centre
ECMWF	European Center for Medium-range Weather Forecasts
EUROGOOS, ROOS Arctic ROOS BOOS NOOS IBI-ROOS MOON Black Sea GOOS	The European Global Ocean Observing System (http://eurogoos.eu/) and its Regional Operational Oceanographic System Arctic Regional Ocean Observing System Baltic Operational Oceanographic System North West Shelf Operational Oceanographic System Iberic-Biscay-Irish Operational Oceanographic System Mediterranean Operational network for the Global Ocean Observing Black sea
NetCDF	Network Common Data Form
CF	Climate and Forecast convention for NetCDF formats
OGS	Istituto Nazionale di Oceanografia e di Geofisica sperimentale https://www.inogs.it/it
NRT	Near Real Time
HCMR	Hellenic Centre for Marine Research
HFR	High Frequency Radar
GDOP	Geometric Dicultion Of Precision
GDAC	Global Data Assembly Centre
DAC	Data Assembly Centre
CODE	Coastal Ocean Dynamics Experiment
CARTHE	Consortium for Advance Research on Transport of Hydrocarbon in the Environment
RTQC / QC	Real Time Quality Control / Quality Control
GDOSA	Geometric Dilution of Statistical Accuracy
ADCP	Acoustic Doppler Current Profiler
EOV	Essential Ocean Variable
SVP	Surface Velocity Program
GTS	Global Telecommunication System
PU	Production Unit

I EXECUTIVE SUMMARY

I.1 Products covered by this document

This document applies to the INSITU_GLO_PHY_UV_DISCRETE_NRT_013_048 product. It consists of a total of four datasets (see **Table 1**), three of which are dedicated to near-surface currents measurements and one dataset with additional sub-surface velocities:

- **cmems_obs-ins_glo_phy-cur_nrt_drifter_irr,** named **drifter** in the rest of the document: near-surface zonal and meridional raw velocities measured by drifting buoys, wind & wind stress components, surface temperature if available (see I.2.1). These surface observations are part of the DBCP's Global Drifter Program but contains also other data sources (OGS data on the Mediterranean Sea, see §II.1)
- **cmems_obs-ins_glo_phy-cur_nrt_radar-total_irr,** named **radar_total** in the rest of the document: near-surface zonal and meridional raw velocities measured by High Frequency radars (HF radars, as acronym HFR), standard deviation of near-surface zonal and meridional raw velocities, Geometrical Dilution of Precision (GDOP), quality flags and metadata. These surface observations are part of the European HF radar Network (see Mader et al., 2017 and Corgnati et al., 2018)
- **cmems_obs-ins_glo_phy-cur_nrt_radar-radial_irr**, named **radar_radial** in the rest of the document: near-surface zonal and meridional components of raw radial velocities measured by High Frequency radars (HF radars, as acronym HFR), magnitude and direction of near-surface zonal and meridional components of raw radial velocities, standard deviation of near-surface zonal and meridional components of raw radial velocities, quality flags and metadata. These surface observations are part of the European HF radar Network (see Mader et al., 2017 and Corgnati et al., 2018)
- **cmems_obs-ins_glo_phy-cur_nrt_argo_irr,** named **argo** in the rest of the document: ocean currents derived from the original trajectory data from Argo GDAC (Global Data Assembly Center). Deep current is calculated from floats drift at parking depth, surface current is calculated from float surface drift.

dataset	cmems_obs-ins_glo_phy-cur_nrt_drifter_irr	cmems_obs-ins_glo_phy-cur_nrt_radar-total_irr	cmems_obs-ins_glo_phy-cur_nrt_radar-radial_ir	cmems_obs-ins_glo_phy-cur_nrt_argo_irr
Equivalent dataset name in following sections	**Drifter**	**radar_total**	**radar_radial**	**Argo**
Geographical coverage	Global	European and US Seas (from coast to up to >200 km depending on the operating frequency)	European Seas (from coast to up to >200 km depending on the operating frequency)	Global
Variables	Zonal and Meridional Velocities at 15-m depth, Surface Temperature if available, Zonal and Meridional wind stress from ECMWF**, Zonal and Meridional 10-m wind from ECMWF** + QC variables + metadata	Zonal and Meridional Velocities at the surface (actual depth depending on the operating frequency), standard deviation of zonal and meridional velocities at the surface Geometrical Dilution of Precision (GDOP) + QC variables + metadata (global attributes)	Zonal and Meridional components, magnitude and direction of radial (referred to the individual measuring HFR stations) velocities at the surface (actual depth depending on the operating frequency), standard deviation of zonal and meridional components of the radial velocities at the surface + QC variables + metadata (global attributes)	Zonal and Meridional Velocities at surface and sub-surface derived from Argo trajectory files with QC variables and metadata.
Available time series	01/01/2002 to present	12/2018 to present		1997 to present
Temporal resolution	1-hour from the 25th of March 2018* 3-hours before the 25th of March 2018*	Typical resolution 1h (exceptions with 15' or 30')		Typical resolution of 10 days
Delivery time	Once a week on Monday	every hour		daily
Horizontal resolution	discrete	*Gridded (Typically ranges from a few hundred meters to 5-6 km, depending on HF Radar operating central frequency and bandwidth*		discrete
Delivery mechanism	Copernicus Marine Service Information Service (with a backup FTP)			
Horizontal resolution	discrete			
Format	NetCDF-4			

Table 1: *List of In Situ TAC datasets for which this document applies*

*In 2017, the algorithm used to compute the currents has been changed to allow the estimation of the 1-hour time resolution field (**For 3-hour** resolution: kriging algorithm from D.V. Hansen et P.M Poulain, given by NOAA/AOML /// **For 1-hour** resolution: Elipot et al 2016 -

http://dx.doi.org/10.1002/2016JC011716; code : https://github.com/selipot/hourly-drifters). Since the 25th of March 2018, the NRT drifters are delivered with this new 1-hour time resolution.

**Furthermore, the ECMWF 10m wind and wind stress components are interpolated at the drifters´ positions and delivered in the drifters' files from the 25th of March 2018 also.

I.2 Summary of the results

I.2.1 Dataset drifter

In some regions and time periods, the number of NRT measurements can be critically low due to the drifter launch time schedule (Figure 1) and their geographical locations (see for example Figure 2 for a 3-month period). The number of drifters has continuously increased from 2003 and reached around 1200 in the last 4 years. The spatial distribution of the measurement is sparse or non-existent in high latitudes. Data ingestion from institutions performing Lagrangian experiments on a regular basis (e.g. Search-and-Rescue Agencies, Universities, Research Institutions) that are not currently considered as data providers, should be explored.

Data availability in the Mediterranean Sea has recently been increased adding information retrieved from INSITU_MED_PHYBGCWAV_DISCRETE_MYNRT_013_035. This dataset includes different drifter designs and also collects data from coastal and/or short-term experiments retrieved from research institutes and international data centres.

In this new version of the product, data from instruments that have lost their drogue (when relevant, as for the SVP platform) are also provided.

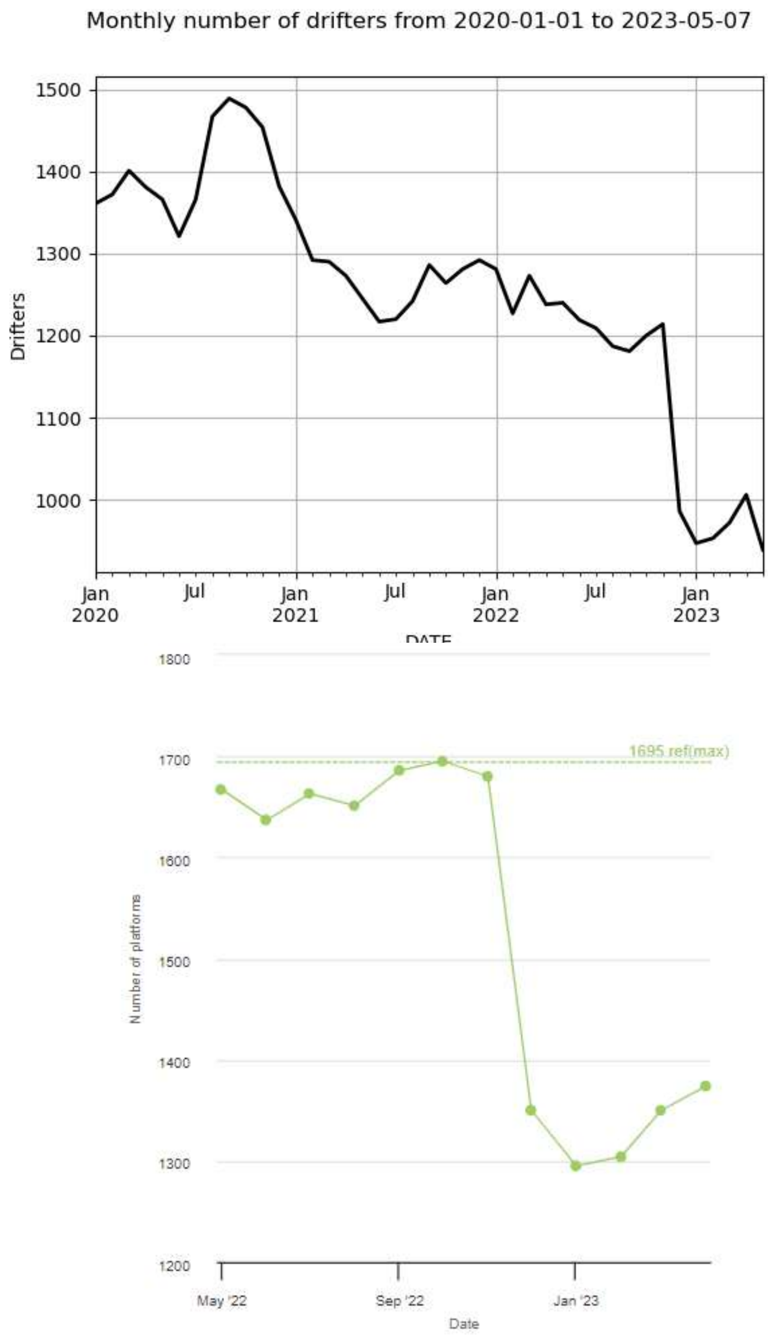

Figure 1: top: Count of transmitting drifters per month from January 2020 to May 2023 with drogue on and, bottom, number of total drifters with and without drogue from May 2022 to May 2023 (from http://www.marineinsitu.eu/monitoring/). Please, be aware that the drifter dataset (DC data) is built from DB data (i.e. displayed bottom), but additional tests are added and the trajectories could differ.

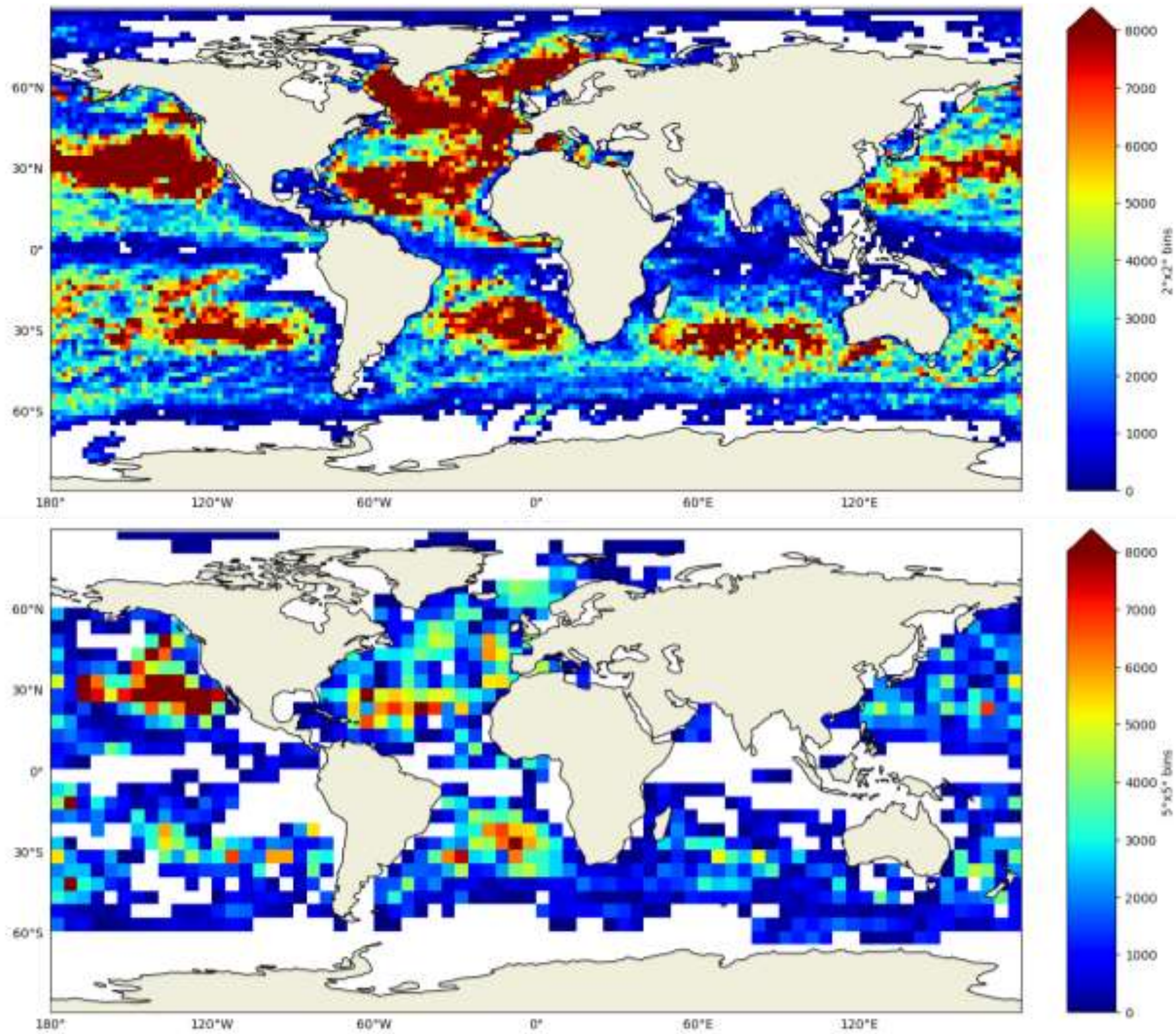

Figure 2: Mean number of measurements from January 2020 to May 2023 (up, 2x2° bins) and over a 3-month period from January 2023 to March 2023 (bottom, 5x5° bins).

I.2.2 Dataset radar_total and radar_radial

The last inventory shows that there are 88 HFRs currently deployed and active in various coastal areas of the European seas (Figure 3, see live map in http://eurogoos.eu/high-frequency-radar-task-team/). This number is growing with seven new HFRs installed per year. The European HFR node delivers in near real-time and at hourly basis, maps of total and radial surface current velocities from the HF radars that are actively processing and/or delivering their (formatted or raw) data to the node.

HFRs are distributed amongst the different Regional Ocean Observing Systems (ROOS) areas coordinated by the European Global Ocean Observing System (EuroGOOS): 49% in MONGOOS (Mediterranean Operational Network for the Global Ocean Observing System), 38% in IBIROOS (Ireland-Biscay-Iberia Regional Operational Oceanographic System) and 13% in NOOS (north West European Shelf Operational Oceanographic System) (Rubio et al., 2017) as shown in Figure 3.

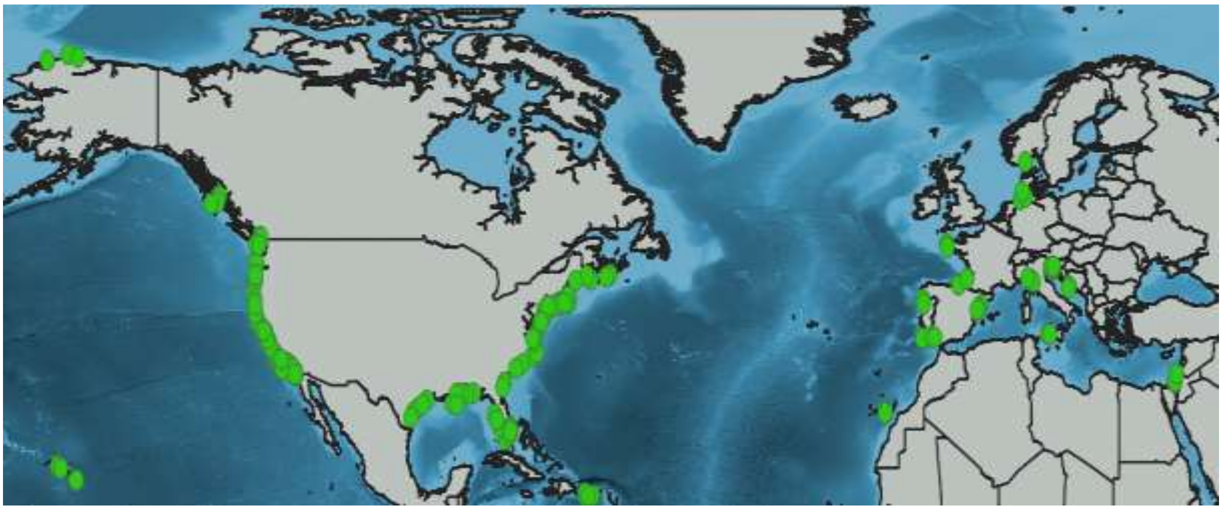

Figure 3: Distribution of the HFR systems contained in the radar_total dataset. European systems are also contained in the radar_radial dataset.

I.2.3 Dataset Argo

The Argo currents dataset is derived from Argo floats trajectories available on Argo GDAC (Global Data Assembly Centre). To provide reliable currents, the dataset considers Argo trajectory files in version 3.1 or higher. In May 2023, the Argo current dataset was assembled from 12 742 floats trajectory files from Argo GDAC, coming from 10 DACs (Data Assembly Centres, see Figure 4). Note that because of obsolete files format and content, around 30% of the 19 345 floats trajectories available in the database cannot be used to calculate currents.

dac	nb floats
AOML	8 001
Coriolis	2 487
JMA	531
Csiro	525
CSIO	519
Meds	319
Incois	193
BODC	95
Kordi	58
NMDIS	14
Total	12 742

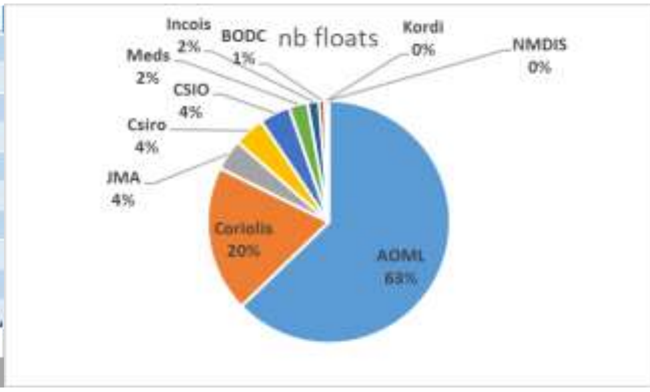

Figure 4: Number of Argo current files, distribution per provider (data assembly centre).

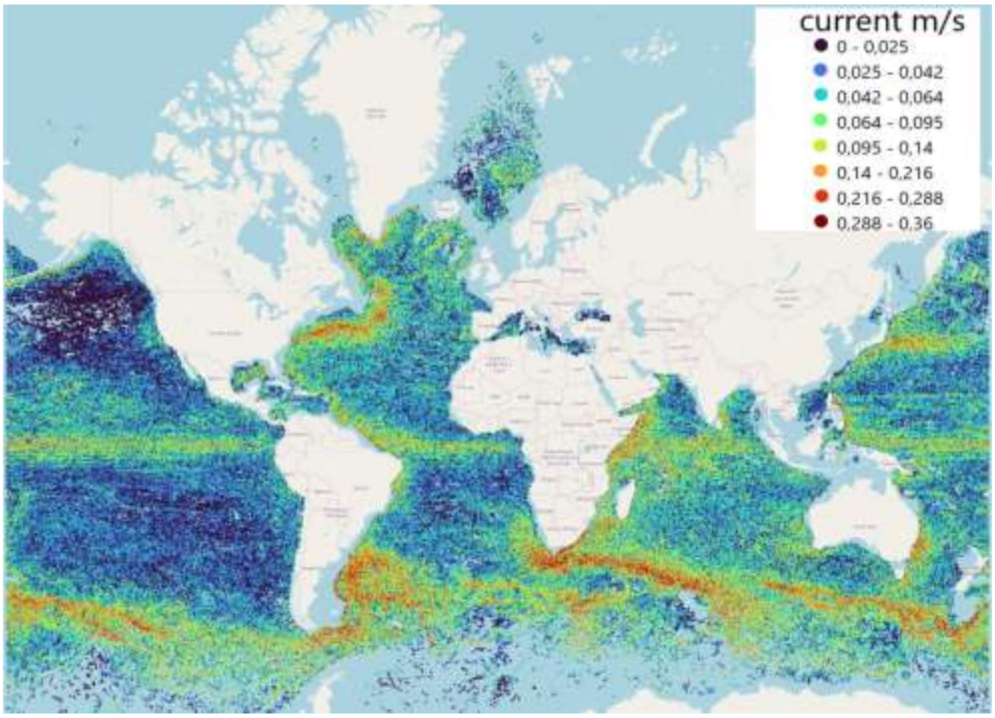

Figure 5: Map of Argo deep ocean currents positions and drifting velocities (Jan 2000 to May 2023), Each dot represents the deep ocean current from one cycle (typically 10 days) from one float .

I.3 Estimated Accuracy Numbers

Table 2 summarizes the accuracy of the measurements depending on platforms and sensors. This is the best accuracy that a user can expect for the data.

Data type	Accuracy	Metrics
Drifter	1 cm/s	Poulain et al., 2012
Radar_total & radar_radial	3–12 cm/s	Liu et al., 2010; Ohlmann et al.; 2007, Molcard et al., 2009; Kalampokis et al., 2016; Lana et al. (2015) ; Lorente et al. 2022
Argo	-	There is no estimated accuracy for Argo currents. Additional research is needed to provide a realistic number; the Argo current is typically the integration of 10 days of parking drift at depth without geo localization

Table 2: Accuracy of the measurements expected from each platform

II PRODUCTION SYSTEM DESCRIPTION

The production centres in charge of the datasets described in the following subsections II.1, II.2 and II.3 are: Coriolis, France for drifter and argo datasets and the European HFR node for radar_total and radar_radial datasets.

II.1 Dataset drifter

Description:

SVP drifters (mainly) and GL_TS_MO files

The Coriolis data Centre delivers every Monday **1-hour (3-hours before the 25th of March 2018)** 15 m depth velocities measurements from drifters.

Most of the drifters are of SVP type (or derived, see Figure 6) and are part of the DBCP's Global Drifter Program which transmits the data in real-time to the Global Telecommunication system (GTS). Their drogue is centred at 15-meter depth. These data are first collected on the GTS, then analysed and pre-processed by the Marine Meteorological Center of Meteo-France (CMM) in the frame of the French project Coriolis, dedicated to operational oceanography in situ observation management.

Other operational qualification (see sec. III) is also done by Coriolis before the final dissemination of the data to Copernicus Marine Service project in Copernicus Marine Service file format (see format in CMEMS-INS-PUM-013_048).

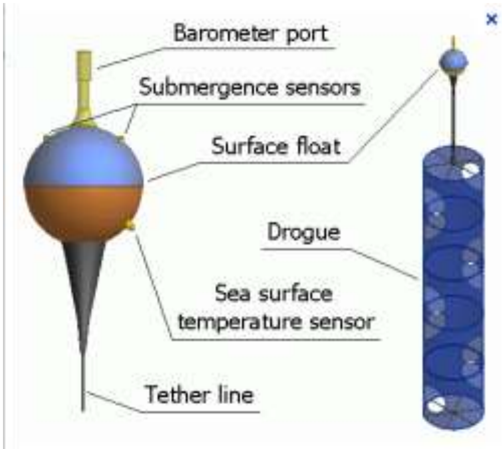

Figure 6: Schematic drawing of an SVP-B type buoy

Drifters processing steps carried out each Monday at CMM on the latest 8 days of data collected (Figure 7):

- Selection and analysis of the data (raw speed threshold test, position quality flag, etc.)
- First test of drogue loss detection from submersion sensor. This information is a critical point essential to use this velocities dataset (representative of the surface currents and not of the wind induced drift if drogue is lost)
- Interpolation of the positions and calculation of the hourly currents from NOAA / AOML method (Elipot et al. 2016).

- Interpolation on each interpolated position of the sea surface temperature if available, as well as of the 6-hour integrated zonal and meridional components of the wind stress and 10-m wind from ECMWF (European Center for Medium-range Weather Forecasts).
- Second analysis of drogue loss detection from model winds and calculated currents (consistency between the 2 signals from spectral analysis & regression analysis).

Figure 7: Production system description for drifter

Note that the tests done to detect the drogue loss are not completely reliable, in fact the methodology used has limitations such as the impact of the sea state on the submersion reference, the sensors behaviour which can differ depending on the manufacturer, the uncertainties as to the date of drogue loss because its removal can take several times to occur, being partial before being complete or the uncertainties in the wind model. Hence it is possible that some of the data provided to Copernicus Marine Service and flagged with drogue attached may correspond to periods when a drifter has instead lost its drogue.

In this new version, both drogued and undrogued drifters are delivered in Copernicus Marine Service. Hence, the user has to refer to the CURRENT_TEST flag to select drogued or undrogued data:

- Drogued data provide velocity information at the drogue center depth (15m for most of them);
- Undrogued data provide velocity information at the surface and can be contaminated by direct wind effect on the float (not linked to ocean current).

The result of the CURRENT_TEST flag is provided in Table 3. Drogue can be considering missing for CURRENT_TEST values equal to 011.

Code	Meaning	Comment
0	Drogue probably missing	These data are not distributed, except for SVP drifters in MO_TS_DC files (Mediterranean Sea dataset, see §I.2.1)
1	Test not performed or not relevant (case for some MO_TS_DC platforms)	-
2	Weak probability of drogue presence	-
3	Strong probability of drogue presence	-

Table 3 : Description of the tests done for drogue loss on SVP drifters

Specificities of the Mediterranean drifters (files MO_TS_DC) of the dataset "drifter"

The OGS Mediterranean drifter dataset consists of drifter data collected in the Mediterranean Sea from various institutions and countries. The raw data are collected and stored, using automatic procedures (pre-processing) executed every morning, and then are decoded and edited (processing). The automatic editing procedure checks positions, times, spike occurrence, drogue presence and associates the appropriate quality flag (real time quality control). Additional validation is carried out every 6 months using a manual editing procedure (delayed time quality control). The automatic editing procedure eliminates the majority of the spikes, nevertheless, some erroneous data require a visual check and the decision of an operator in order to be removed (e.g. large temporal gaps along the drifter trajectories or strandings). Edited data are interpolated at 30 minutes uniform intervals using a kriging optimal interpolation method (Hansen and Poulain, 1996). The velocities are then calculated as finite differences of the interpolated position, and data are finally subsampled at 1 hour. Many drifters distributed through the MO_TS_DC files, such as CODE or CARTHE, are considered to not have any drogue. These measurements can be considered to be surface observations. For these buoys, the tests on the drogue loss are not activated. These tests are done for SVP drifters only (see description of the quality flags and tests in the CMEMS-INS-PUM-013_048 document of the product).

As an example, CODE drifters consist of a slender, vertical, 1-m-long negatively buoyant tube with four drag-producing vanes extending radially from the tube over its entire length and four small spherical surface floats attached to the upper extremities of the vanes to provide buoyancy. Comparisons with current meter measurements and studies using dye to measure relative water movements showed that the CODE drifters follow the surface currents to within 3 cm/s, even during strong wind conditions (Menna et al, 2017). More information on these data and their pre-processsing and validation can be found in the publications [Menna et al., 2017, all instruments: content of the Mediterranean drifters OGS database] and [Menna et. al 2018, SVP drogue loss detection method]. Drifter data are sent to the Distribution Unit every day and every month. History files are produced sporadically and are updated by HCMR who collaborates with OGS when manual editing is carried out .

II.2 Dataset radar_total and radar_radial

HFR is a land-based remote sensing technology (see Figure 8) that has been shown to be a cost-efficient tool to monitor coastal regions at a range of up to 200 km. Oceanographic HFRs are mainly utilized to measure ocean surface current fields for various applications such as search and rescue, oil spill monitoring, marine traffic information or improvement as well as data assimilation of numerical circulation models [Paduan and Rosenfeld, 1996; Gurgel et al., 1999; Rubio et al. 2018, Reyes et al., 2022].

HFRs rely on resonant backscatter resulting from coherent reflection of the transmitted wave by the ocean waves whose wavelength is half of that of the transmitted radio wave. This phenomenon is known as Bragg scattering, and it results in the first order peak of the received (backscattered) spectrum (Paduan and Graber, 1997). The difference between the theoretical speed of the waves and the velocity observed, resulting in the Doppler shift in the observed Bragg peaks, is due to the velocity of the radial component of the current (the current in the same direction of the signal), that can be therefore estimated.

HFRs belong to the remote sensing instruments family. Based on the analysis of the electromagnetic waves (in the high frequency band) back scattered by the ocean surface and the associated doppler shift, each radar station is able to determine the radial component of the surface current velocity, i.e. the component of the velocity along the radial direction away from -negative- or towards -positive- the radar antenna itself, for each cell of a given polar grid, determined by the angular/radial resolution and max range of the instrument. Each HFR station produces then a two-dimensional map on a polar grid containing the radial surface current velocity (radar_radial). To obtain complete information, i.e. total surface current vectors (radar_total), data from at least two HFR stations with overlapping coverage must be combined. Total velocities are calculated using unweighted least square fit that maps radial velocities measured from individual sites onto a cartesian grid. The final product is a map of the horizontal components of the ocean surface currents on a regular grid in the area of overlap of two or more radar stations (see example in Figure 9).

HFRs provide current data only relative to the surface within an integration depth ranging from tens of centimetres to 1-2 meters depending on the operating central frequency. These data (radar_total and radar_radial) are first collected by the European HF Radar Node and then verified and (when necessary) post-processed before being transferred to the Copernicus Marine Service In Situ TAC Global Production Unit.

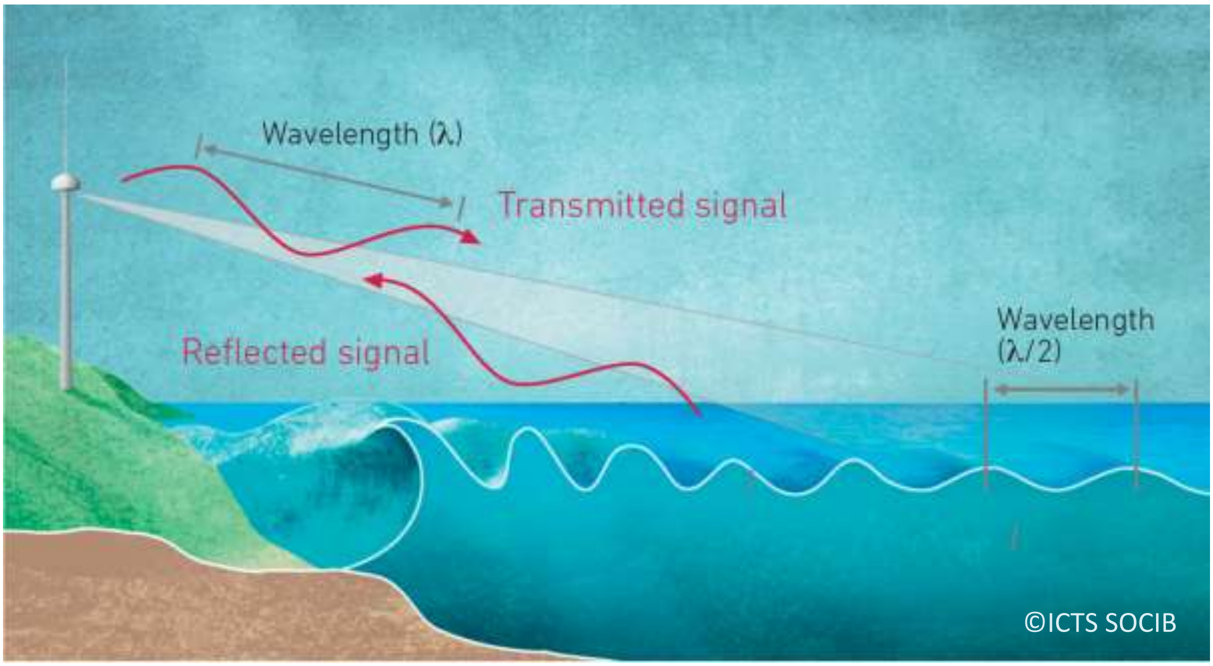

Figure 8: HF radar's principle of operation (adapted from Barrick et al., 1977).

The European HFR Node acts as the focal point for the European HFR data providers and implements the HFR data stream from the data providers to the Copernicus Marine Service In Situ TAC Global Production Unit (PU).

The European HFR Node delivers every hour zonal and meridional current velocity gridded fields at the near-surface (actual depth depending on the operating frequency), i.e. radar_total dataset, and zonal and meridional components and magnitude and direction of radial (referred to the individual measuring HFR stations) current velocities at the surface (actual depth depending on the operating frequency), i.e. radar_radial dataset.

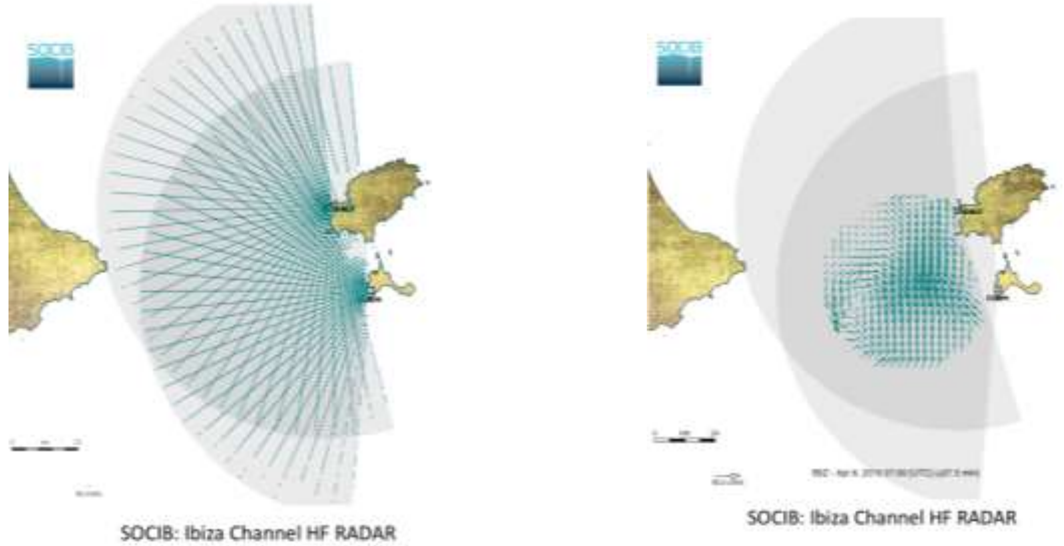

Figure 9: Maps of HFR radial velocities for two radial sites, showing the radial coverage (left) and total surface velocities in the overlapping area (right).

The delivery dataflow is structured as follows:

- if the data provider can generate HFR data according to the defined data format and QC standards, the node only collects and checks the radial and total data and pushes them to the Global PU.
- If the data provider cannot generate HFR data according to the defined data format and QC standards, the HFR Node harvests the radial and total raw data from the provider, harmonizes, quality-controls, formats the data and pushes them to the Global PU.

The strength and flexibility of this solution reside in the architecture of the European HFR node, that is based on a centralized database, fed both by the operators via a webform and by the software routines running on the node, containing updated metadata of the HFR networks and the needed information for processing, quality-controlling and archiving the data (schematized in Figure 10). A set of shared software tools uses all that information for processing native HFR data for quality controlling and converting them to the standard format for distribution. This strategy guarantees that, whatever the workflow, the data are processed by the same software tools.

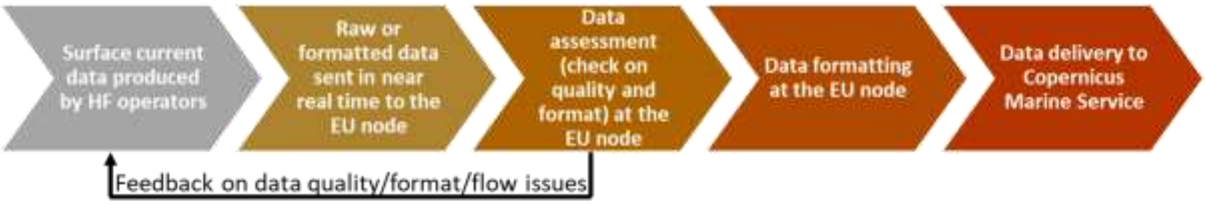

Figure 10: Schematic view of the production system description for HFR total and radial datasets.

II.3 Dataset Argo

The Argo current product produced by Copernicus In Situ TAC is derived from the original trajectory data from Argo GDAC (Global Data Assembly Center), available at: ***Argo float data and metadata from Global Data Assembly Centre (Argo GDAC)***, *SEANOE (https://doi.org/10.17882/42182).*
In 2022, the GDAC distributed data from more than 16,000 Argo floats. Deep ocean current is calculated from floats drift at parking depth, surface current is calculated from float surface drift. The ocean current product contains a NetCDF file per Argo float. It is updated daily in real time by automated processes.

The Argo currents are produced from Argo trajectories format version 3.1 or higher (12˙742 floats in August 2022); the previous formats are ignored (2.*, 3.0).

For the November 2023 release, two major improvements are implemented:

- A series of 20 quality control tests is applied on each Argo trajectory file (Table 4)
- The currents are calculated with the Ollitrault-Rannou method documented in Herbert Gaelle (2020).

Test n°	category	name
1	Cycle	Double cycle anomaly
2	Cycle	Non monotonic cycle number
3	Cycle	Cycle duration anomaly
4	Cycle	Missing cycle anomaly
5	Location	Invalid date
6	Location	Invalid position
7	Location	Invalid start location date
8	TS	Invalid temperature
9	TS	Invalid salinity
10	Pressure	Invalid pressure
11	Grounded	Isas pressure comparison
12	Individual cycle	Date duplicate
13	Individual cycle	Non monotonic date
14	Individual cycle	Invalid duration between location
15	Individual cycle	Invalid cycle duration
16	Deployment	First location anomaly
17	Deployment	Missing cycle 0
18	Position	Invalid position
19	Drift	Drift duration anomaly
20	Drift	Kobayashi position anomaly

Table 4: Additional control tests applied to Argo trajectory files

Typical Argo float behaviour

An Argo float drifts freely in the global ocean, performing regular observation cycles of the water column by changing its buoyancy (Figure 11).

An observation cycle is usually spread over 10 days and consists of:

- a descent from the surface to a parking depth (generally 1500 meters deep)
- a roughly 9.5 days drift at this parking depth over the 10-day total cycle time
- an ascent to the surface (vertical profile)
- A short surface drift for data transmission the duration of which depends on the positioning systems. Argo floats that use the Argos satellite system need to stay almost half a day at the surface to transmit, whereas it takes less than half an hour for Iridium.

The data transmitted at each cycle contain temperature, salinity observations (and additional biogeochemical parameters if applicable), positions (gps or argos), and additional technical data.

The parking depth information comes from the RPP Representative Park Pressure (RPP) of the float cycle. It can vary with each cycle. The RPP is provided in the original trajectory file.

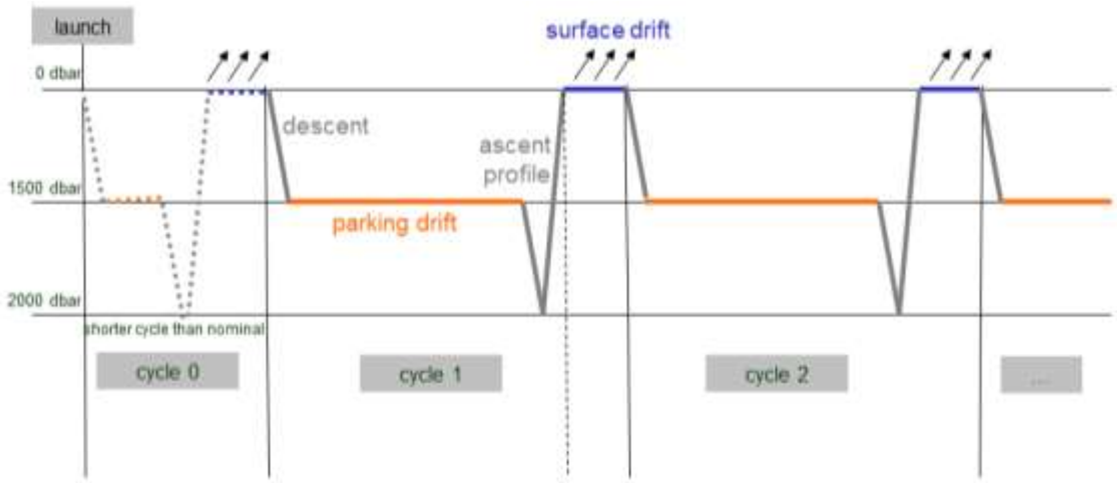

Figure 11: The cycles of an Argo float.

Velocity calculation

The positions used to estimate the velocities are measured during the surface drift (Argos or GPS positioning, no Iridium):

- For the surface current of cycle N, the first and last good position of the N cycle are considered (Figure 12).
- For the deep current of cycle N, the last good position of cycle N-1 and the first good position of cycle N are considered (Figure 12).

The current vector is positioned and dated at the last position of the N-1 cycle. For more details on the method, the user can refer to to the publication *Ollitrault et al (2013*

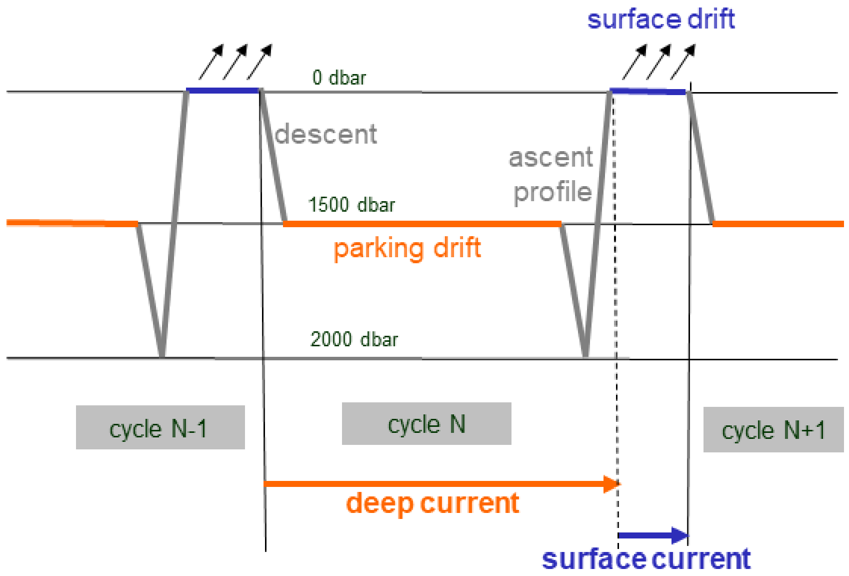

Figure 12: Deep and surface current. The deep current mainly represents the 10 days parking drift of a float cycle, the surface current is the surface drift (a few hours) of a float cycle

III VALIDATION FRAMEWORK

The In Situ TAC is dedicated to assuring the accuracy of in situ observations. This consists of the Real Time Quality Control (RTQC) of the in-situ observations.

III.1 Dataset drifter

For the drifters, the qualification is done at first stage by Meteo-France during preprocessing of the data from the GTS (outliers detection, position on land, drogue loss, as illustrated in sec. II.1) and in a second stage by Coriolis, which applies the Real Time Quality Control (RTQC) [*EuroGOOS DATA-MEQ working group (2010).*]. These metrics can be subject to change in some details. The mandatory metrics for application are:

- Platform identification
- Impossible date
- Impossible location
- Position on land
- Spike

Furthermore, the quality of the dataset, and not of the data values, is monitored also through the estimation of several Key Performance Indicators (KPIs) (http://www.marineinsitu.eu/monitoring/):

- Timeliness of delivery
- Number of platforms per day
- Data quality flag percentages during specified period in months
- Parameters

III.2 Dataset radar_total

The European HFR Node is in charge of checking the validity of the HF radar data files and of applying the RTQC in compliance with the EU common data and metadata Standard for HF radar surface current data.

Mandatory NRT QC tests, listed below, are applied to the total surface current data (radar_total) according to the European common QC standard for NRT HFR current data. These metrics are subject to change in some details.

- **Syntax check**: this test will ensure the proper formatting and the existence of all the necessary fields within the total NetCDF file. This test is performed on the NetCDF files and it assesses the presence and correctness of all data and attribute fields and the correct syntax throughout the file. This test is performed by the European HFR Node before pushing data to the distribution platforms.
- **Data Density Threshold**: this test labels as good data the total velocity vectors with a number of contributing radials bigger than the threshold and as bad data the total velocity vectors with a number of contributing radials smaller than the threshold.
- **Velocity Threshold**: this test labels as bad data the total velocity vectors whose module is bigger than a maximum velocity threshold and as good data the total vectors whose module is smaller than the threshold.

- **Variance Threshold**: this test labels as bad data the total vectors whose temporal variance is bigger than a maximum threshold and as good data the total vectors whose temporal variance is smaller than the threshold. This test is applicable only to Beam Forming (BF) systems. Data files from Direction Finding (DF) systems will apply instead the "Temporal Derivative" test reporting the explanation "Test not applicable to Direction Finding systems. The Temporal Derivative test is applied." in the comment attribute.
- **Temporal Derivative**: for each total bin, the current hour velocity vector is compared with the previous and next hour ones. If the differences are bigger than a threshold (specific for each grid cell and evaluated on the basis of the analysis of one-year-long time series), the present vector is flagged as "bad data", otherwise it is labelled with a "good data" flag. Since this method implies a one-hour delay in the data provision, the current hour file should have the related QC flag set to 0 (no QC performed) until it is updated to the proper values when the next hour file is generated.
- **GDOP Threshold**: this test labels as bad data the total velocity vectors whose GDOP (Geometrical Dilution Of Precision) is bigger than a maximum threshold and as good data the the vectors whose GDOP is smaller than the threshold.

These mandatory QC tests are manufacturer-independent, i.e. they do not rely on particular variables or information provided only by a specific device, and they are required for labeling the HFR total velocity data as Processing Level 3B (Level 3A data that have been processed with a minimum set of QC)[1] as detailed in Table 7.

For some of these tests, HFR operators will need to select the best thresholds. Since a successful QC effort is highly dependent upon selection of the proper thresholds, this choice is not straightforward, and requires a trial-and-error approach, based on historical knowledge or statistics derived from historical data, before the final selections are made.

[1] Please refer to Appendix A of the JERICO-NEXT deliverable D5.14 "Recommendation Report 2 on improved common procedures for HFR QC analysis" for the processing level definition (as summarized in Table 12; http://www.jerico-ri.eu/download/jerico-next-deliverables/JERICO-NEXT-Deliverable_5.14_V1.pdf).

Processing Level	Definition	Products
LEVEL 0	Reconstructed, unprocessed instrument/payload data at full resolution; any and all communications artifacts, e.g. synchronization frames, communications headers, duplicate data removed.	Signal received by the antenna before the processing stage. (No access to these data in Codar systems)
LEVEL 1A	Reconstructed, unprocessed instrument data at full resolution, time-referenced and annotated with ancillary information, including radiometric and geometric calibration coefficients and georeferencing.	Spectra by antenna channel
LEVEL 1B	Level 1A data that have been processed to sensor units for next processing steps. Not all instruments will have data equivalent to Level 1B.	Spectra by beam direction
LEVEL 2A	Derived geophysical variables at the same resolution and locations as the Level 1 source data.	HFR radial velocity data
LEVEL 2B	Level 2A data that have been processed with a minimum set of QC.	HFR radial velocity data
LEVEL 2C	Level 2A data that have been reprocessed for advanced QC.	Reprocessed HFR radial velocity data
LEVEL 3A	Variables mapped on uniform space-time grid scales, usually with some completeness and consistency	HFR total velocity data
LEVEL 3B	Level 3A data that have been processed with a minimum set of QC.	HFR total velocity data
LEVEL 3C	Level 3A data that have been reprocessed for advanced QC.	Reprocessed HFR total velocity data
LEVEL 4	Model output or results from analyses of lower level data, e.g. variables derived from multiple measurements	Energy density maps, residence times, etc.

Table 5: HFR data Processing Levels

Furthermore, the quality of the dataset is being monitored through the estimation of several Key Performance Indicators (KPIs) and available in http://www.marineinsitu.eu/monitoring/. The following KPIs are applicable to radar_total dataset (per type, per PU, per parameter):

- Number of platforms over the last month, the last year, and since the beginning of the mission
- Number of providers
- Number of files
- Delay of arrival during the last week (%) and the last month (%)
- Number of platforms in the DU within a day per type
- Number of platforms in the DU within a day per parameter
- Data quality flag percentages per parameter during specified period in months.

In addition, a specific KPI is used to monitor the spatio/temporal coverage of the data in the dashboard of http://www.marineinsitu.eu/dashboard/ (Figure 13).

Performance metrics for **HFR-EUSKOOS-Total**

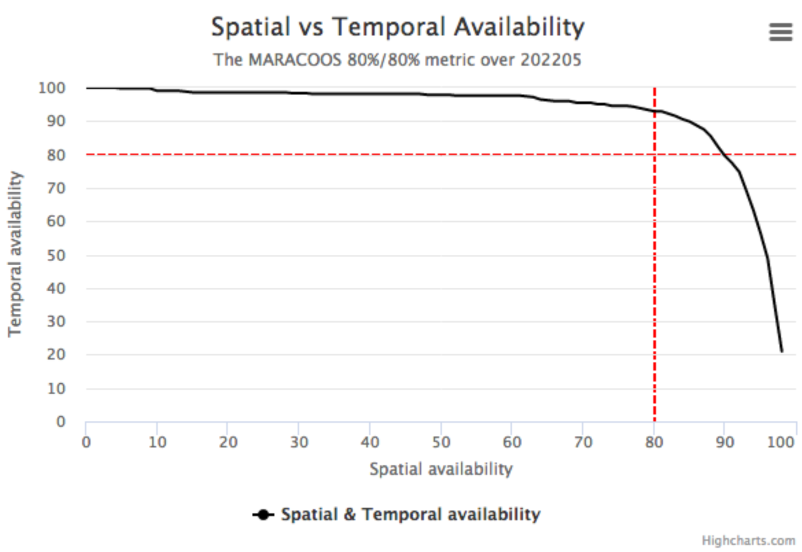

Further reference at: MARACOOS 80%/80% metric

Figure 13: The ratio of spatial and temporal coverage of the HFR-EUSKOOS surface current maps (black line). The data delivery target of the network for 80% spatial coverage at least 80% of the time (dashed red line).

III.3 Dataset radar_radial

The European HFR Node is in charge of checking the validity of the HF radar data files and of applying the RTQC in compliance with the EU common data and metadata Standard for HF radar surface current data.

Mandatory NRT QC tests, listed below, are applied to the radial surface current data (radar_radial) according to the European common QC standard for NRT HFR current data. These metrics are subject to change in some details.

- **Syntax check**: this test will ensure the proper formatting and the existence of all the necessary fields within the radial NetCDF file. This test is performed on the NetCDF files and it assesses the presence and correctness of all data and attributes fields and the correct syntax throughout the file. This test is performed by the European HFR Node before pushing data to the distribution platforms.
- **Over water**: This test labels radial vectors that lie on land with a “bad data” flag and radial vectors that lie on water with a “good data” flag.
- **Velocity Threshold**: this test labels radial velocity vectors whose module is bigger than a maximum velocity threshold with a “bad data” flag and radial vectors whose module is smaller than the threshold with a “good data” flag.
- **Variance Threshold**: this test labels radial vectors whose temporal variance is bigger than a maximum threshold with a “bad data” flag and radial vectors whose temporal variance is smaller than the threshold with a “good data” flag. This test is applicable only to Beam Forming (BF)

systems. Data files from Direction Finding (DF) systems will apply instead the "Temporal Derivative" test reporting the explanation "Test not applicable to Direction Finding systems. The Temporal Derivative test is applied." in the comment attribute.

- **Temporal Derivative**: for each radial bin, the current hour velocity vector is compared with the previous and next hour ones. If the differences are bigger than a threshold (specific for each radial bin and evaluated on the basis of the analysis of one-year-long time series), the radial vector is flagged as "bad data", otherwise it is labeled with a "good data" flag. Since this method implies a one-hour delay in the data provision, the current hour file should have the related QC flag set to 0 (no QC performed) until it is updated to the proper values when the next hour file is generated.
- **Median Filter**: for each source vector, the median of all velocities within a radius of <RCLim> and whose vector bearing (angle of arrival at site) is also within an angular distance of <AngLim> degrees from the source vector's bearing is evaluated. If the difference between the vector's velocity and the median velocity is greater than a threshold, then the vector is labeled with a "bad_data" flag, otherwise it is labeled with a "good_data" flag.
- **Average Radial Bearing**: this test labels the entire data file with a 'good_data" flag if the average radial bearing of all the vectors contained in the data file lies within a specified margin around the expected value of normal operation. Otherwise, the data file is labeled with a "bad_data" flag. The value of normal operation has to be defined within a time interval when the proper functioning of the device is assessed. The margin has to be set according to site-specific properties. This test is applicable only to DF systems. Data files from BF systems will have this variable filled with "good_data" flags (1) and the explanation "Test not applicable to Beam Forming systems" in the comment attribute.
- **Radial Count**: test labeling the entire data file having a number of radial velocity vectors bigger than the threshold with a "good data" flag and data file having a number of radial velocity vectors smaller than the threshold with a "bad data" flag.

These mandatory QC tests are manufacturer-independent, i.e. they do not rely on particular variables or information provided only by a specific device and they are required for labeling the HFR radial velocity data as Level 2B (Level 2A data that have been processed with a minimum set of QC)[2] as detailed in Table 7.

For some of these tests, HFR operators will need to select the best thresholds. Since a successful QC effort is highly dependent upon the selection of the proper thresholds and this choice is not straightforward, a significant trial and error effort is required before final selection is made. These thresholds are not determined arbitrarily but based on historical knowledge or statistics derived from historical data.

Furthermore, the quality of the dataset is being monitored through the estimation of several Key Performance Indicators (KPIs) and is available in http://www.marineinsitu.eu/monitoring/ in the detailed view of the product. The following KPIs are applicable to radar_radial dataset (per type, per PU, per parameter):

[2] Please refer to Appendix A of the JERICO-NEXT deliverable D5.14 "Recommendation Report 2 on improved common procedures for HFR QC analysis" for the processing level definition (as summarized in Table 12; http://www.jerico-ri.eu/download/jerico-next-deliverables/JERICO-NEXT-Deliverable_5.14_V1.pdf).

- Number of platforms, within a day, over the last month, last year and since the beginning of the mission
- Number of providers
- Number of files
- Delay of arrival during the last week
- Data quality flag percentages per parameter during specified period in months.

In addition, a specific KPI is used to monitor the spatio/temporal coverage of the data in the dashboard of http://www.marineinsitu.eu/dashboard/.

III.4 Dataset argo

The Argo trajectory files are quality controlled according to the "Argo quality control manual for CTD and trajectory data" http://dx.doi.org/10.13155/33951
Only good trajectory data (QC = 1) are considered in Argo currents dataset.
Four automated the real-time quality controls applied are:

- Bathymetry test (pressure is above GEBCO 2020 bathymetry)
- Global range speed test (current speed is less than 3 m/s)
- Positive pressure (pressure is >= 0 decibar)
- If the cycle's "GROUNDED" flag is set ("Y"), the current is flagged false.

The Quality Control (QC) flags of the values which fail the test are set to "bad data" (QC = 4).

The additional quality control on trajectories is documented in *Herbert Gaelle (2020)* (document in French only).

IV VALIDATION RESULTS

IV.1 Drifter dataset

For the “drifter” dataset, the KPIs are available on http://www.marineinsitu.eu/monitoring/

The validation tests applied to drifters, described in sec. II.1, resulted in the elimination of 10% of the data from the drifters database in average (erroneous position or speed). Around 30% of the buoys have a drogue loss detection.

IV.2 Radar datasets

The metrics for radar_total and radial_radar data set performance are:

- **Spatial coverage Spatial coverage** - Map of the percent of availability of raw radar_radial or radial_total data in each grid point. The contour shows the area of temporal availability greater than 80% for the last 30 days. The maps are computed for each station independently.
- **Temporal coverage** - Overview of the evolution of the number of platforms providing data for an Essential Oceanic Variable during a certain period of time.

Different steps have been followed for the assessment of the radar_total and radar_radial data uncertainty. As described by Lipa (2013), if we assume that the radar hardware is operating correctly, different sources of uncertainty can be identified in the radial velocities, namely: (a) variations of the radial current component within the radar scattering patch; (b) variations of the current velocity field over the duration of the radar measurement; (c) errors/simplifications in the analysis (e.g. incorrect antenna patterns or errors in empirical first order line determination); (d) statistical noise in the radar spectral data, which can be due to power-line disturbances, radio frequency interferences, ionosphere clutter, ship echoes, or other environmental noise (Kohut and Glenn, 2003). When dealing with total currents, additional geometric errors can affect the accuracy of the HFR data. These errors (GDOP and GDOSA) are distributed spatially and can be controlled and estimated in the processing from total to radials (Chapman et al., 1997; Barrick, 2002).

The EU HFR Node is in charge of checking the validity of the HF radar data files and of applying the RTQC in compliance with the EU Standard for HF radar surface current data. The mandatory metrics for application according to the European common QC standard for NRT HFR current data are summarized in section III.

The evaluation of the radar_total and radar_radial data set uncertainties has been performed mainly through the comparison of HFR data with surface or subsurface drifters, and or in-situ ADCP or current meter measurements in the corresponding HFR footprint areas. These validation exercises can be limited by the fact that part of the discrepancies observed through these comparisons are due to the specificities and own inaccuracies of the different measuring systems. Several examples are provided here for three different areas: the Gulf of Manfredonia (Figure 14), the Ibiza Chanel () and the south-eastern Bay of Biscay (Figure 20). For the Gulf of Manfredonia area, please be aware that the validation results are only given here to illustrate the kind of metrics used to evaluate the quality of the data as this network was only operational over the period 2013-2015 and so is not delivered in the NRT product. These metrics will be replaced in the next version of the QUID by a full analyse of the HFR-TirLig network that is currently being carried out.

Gulf of Manfredonia

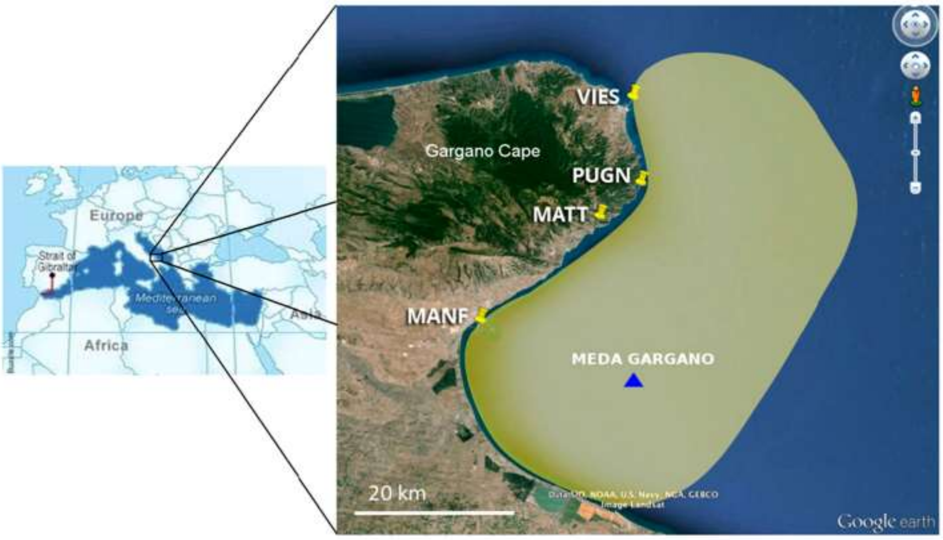

Figure 14: Gulf of Manfredonia

This validation exercise has been done with historical data (HFR-GoM network) for the period 2013–2015 (Corgnati et al., 2018). Note that , even if this network was active before 2018, its data are distributed in the Copernicus Marine Service INSITU_GLO_PHY_UV_DISCRETE_NRT_013_048 product. The network consisted of four HF radars that provided hourly sea surface velocity data in real-time mode. The QC procedures applied to HFR radial velocities are an over-water flag, a radial count threshold and a velocity threshold. The QC procedures applied to HFR total velocities are a velocity threshold and a GDOP threshold. Thus, these data were not processed for all the mandatory QC tests defined by the European common QC model.

HFR radial and total velocity data were compared with in situ velocity measurements by Global Positioning System tracked surface drifters deployed within the radar footprint. The results show a good agreement, with the root mean square (rms) of the difference between radial velocities from HFR and drifters ranging between 20% and 50% of the drifter velocity rms (see Table 6).

Two comparison experiments have been carried out, one in November 2013 against 7 CODE drifters, and the other in February 2014, against 5 CODE drifters.Velocities from HFRs and from drifters are compared at the same times and locations. Drifter data are resampled on the uniform radar time grid, and the radar velocity is estimated through bilinear interpolation of the radar velocities corresponding to the cells closest to each drifter position. The difference between the two estimated radial velocities is then calculated. The statistics of the comparison are evaluated by averaging over all drifter positions at all times in terms of bias μ, root-mean-square differences rms^R_d and zero-lag correlation coefficients ρ_0^2 (Table 6).

Site code	t_d [hours]		rms_d^R [m/s]		$rmse$ [m/s]		μ [m/s]		ρ_0^2	
	Nov	Feb	Nov	Feb	Nov	Feb	Nov	Feb	Nov	Feb
MANF	68	581	0.15	0.12	0.06 (0.05)	0.05 (0.06)	0 (0.02)	0.01 (0.02)	0.80 (0.83)	0.89 (0.82)

Table 6: From Corgnati et al. 2018, results of the comparison between HFR and drifter velocities in the November 2013 and February 2014 experiments. For each value, the corresponding value evaluated without applying the measured antenna pattern is reported in parenthesis. Rms of the velocities sensed by the drifters rms^R_d and time t_d spent by all the drifters within each radar coverage are reported as well.

For all sites and both experiments, the calibrated rmsd lies in the range 0.03–0.08 m/s, well within what is considered acceptable in the literature (Sentchev et al., 2017)

The HFR data have also been compared with subsurface velocity profiles from an upward looking acoustic Doppler current profiler (ADCP) during winter 2015, to gain information on the correlation between surface and water column velocities. This information is especially relevant for fishery and coastal management applications, where transport of larvae, sediments, and pollutants in the water column are considered.

In order to verify whether the HFR information can be considered representative of the water column behaviour, the comparison between HFR surface velocity and ADCP velocity in the Gulf was performed, concentrating on two periods during January and March 2015, when both measurements were available in the Gulf. The considered ADCP measures zonal and meridional components of water velocity in three depth cells spanning 5 m of the water column each, with an accuracy of 0.005 m/s. Cell 1 covers the depth range 1–6 m from surface, cell 2 covers the depth range 6–11 m from surface, and cell 3 covers the depth range 11–16 m from surface. The first meter under the surface is not covered by any cell to avoid interferences caused by tides and waves. Water velocity measurements are sampled every 10 min in each cell.

The zonal and meridional components of the total velocities from HFRs and the zonal and meridional components of water velocities measured at each depth level from the ADCP are compared at the same time and locations. On the HFR side, velocity components in the grid cell where the ADCP is located are extracted for comparison along the time series. The 10-min velocity components measured by the ADCP are averaged, separately for each depth cell, on the corresponding 1-h intervals. Table 7 shows the maximum cross correlations ρ^2 and the corresponding time lags τ evaluated for the zonal and meridional components of water velocity measured by the ADCP between adjacent depth levels from sea surface for the two periods January 1-12, 2015 and March 1-11, 2015.

Depth cell (m from surface)	$\rho^2_{u\_ADCP}$		$\rho^2_{v\_ADCP}$		τ_{u_ADCP} [hours]		τ_{v_ADCP} [hours]	
	Jan	Mar	Jan	Mar	Jan	Mar	Jan	Mar
Cell 1 ([1-6] m) vs Cell 2 ([6-11] m)	0.97	0.94	0.98	0.99	0	-1	0	1
Cell 2 ([6-11] m) vs Cell 3 ([11-16] m)	0.91	0.94	0.98	0.98	5	3	0	1

Table 7: From Corgnati et al. 2018, maximum cross correlations ρ^2 and the corresponding time lags τ evaluated for the zonal and meridional components of water velocity measured by the ADCP between adjacent depth levels from sea surface for the two periods January 1-12, 2015 and March 1-11, 2015 – Gulf of Manfredonia.

Depth cell (m from surface)	ρ^2_u		ρ^2_v		τ_u [hours]		τ_v [hours]	
	Jan	Mar	Jan	Mar	Jan	Mar	Jan	Mar
Cell 1 ([1-6] m)	0.83	0.76	0.95	0.95	-4	-10	0	1

Table 8: From Corgnati et al. 2018, maximum cross correlations ρ^2 and the corresponding time lags τ evaluated between HFR and ADCP zonal and meridional components of water velocity at the surface level (1-6 m from surface) for the two periods January 1-12, 2015 and March 1-11, 2015 - Gulf of Manfredonia.

Results show that, at least in the considered periods, the velocity in the water column is well correlated, and there is a good agreement between surface HFR and ADCP data, with correlations between 0.95 and 0.75 (Table 8).

Ibiza Channel

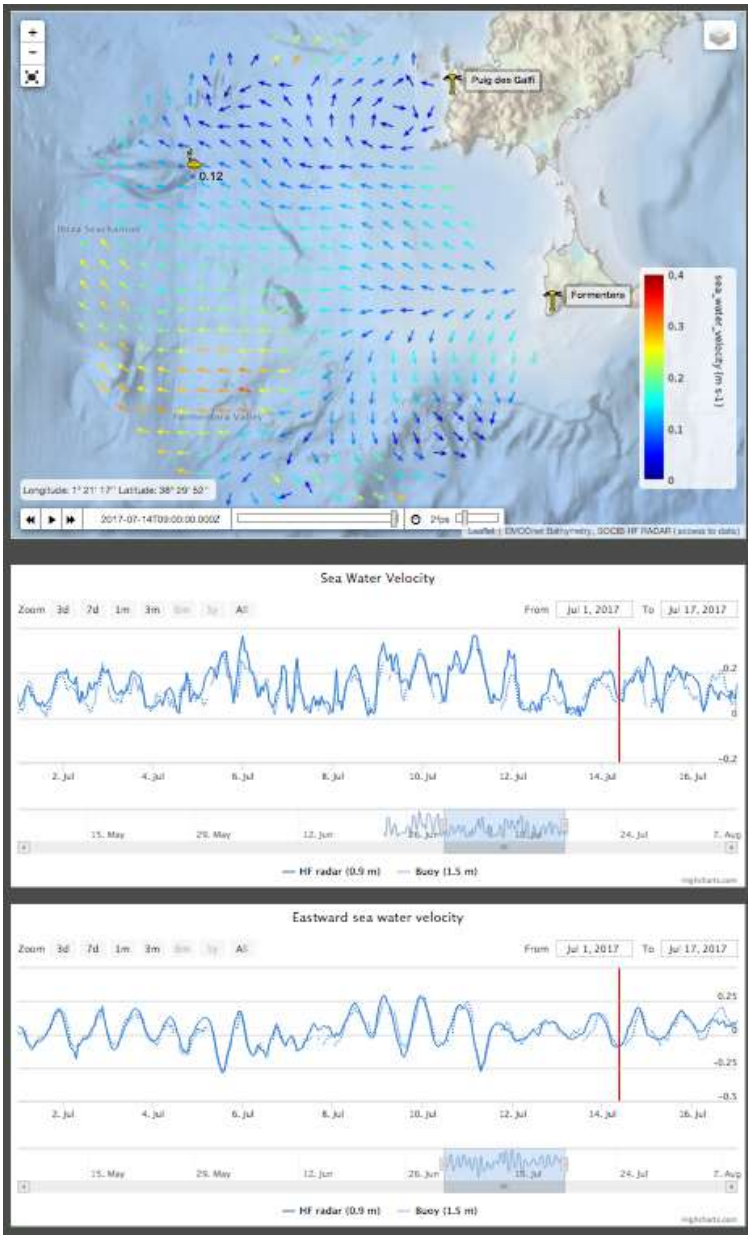

Figure 15: Near-real time validation of the HF radar surface currents (solid line) vs. near-surface currents (dashed line) from a point-wise current meter located in the Ibiza Channel Buoy (moored inside the HF radar spatial coverage)

In the Ibiza Channel some of the validation exercises performed are being done in real-time: the HF radar surface currents (~0.9 m) were systematically compared against current meter measurements from the subsurface point-wise current-meter (1.5 m) located on the Ibiza Channel buoy, moored inside the HF radar total footprint (as shown in) from 2013-09-26 until 2018-05-18. . Assessment of operational HFR total velocities is performed in the Eulerian framework as described in Lana et al. (2016) and following a Lagrangian approach in Révelard et al., (2021) using trajectories of satellite-tracked drifters available in the Ibiza Channel from the experiments carried out in September-October 2014, July-August (2016) and November (2018).

Near real-time validation allows the data provider to perform an operational data assessment, and it allows the identification of gaps (used as an early outage's warning) and/or data anomalies (either from the HF radar system or from the current meter) and the detection of instruments malfunction periods.

In addition to the near-real time validation, validation of HF radar surface currents has been performed against observations from the subsurface point-wise current-meter (depth=1.5m) and from the first bin of the ADCP (depth=5m). Different kind of plots (Quantile-Quantile; Regression plot; qualitative time-series with comparisons; time-series of QC values for both instruments) and statistical metrics have been obtained as in to Figure 19. The results show a high agreement between HFR currents and subsurface currents from current meters and ADCP, at least for the periods considered. For example, the correlation between HFR and ADCP current data ranges from 0.68 to 0.90.

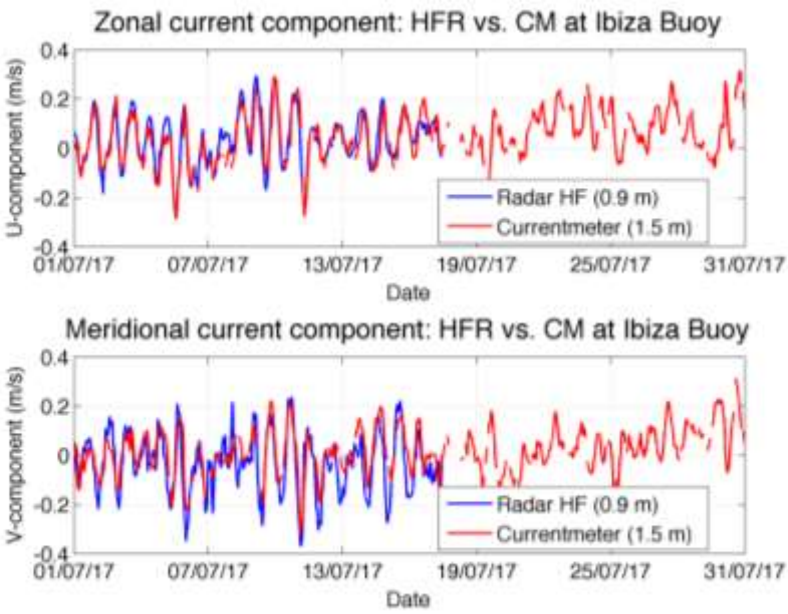

Figure 16: Comparative time-series of zonal (top panel) and meridional (bottom panel) surface current velocity components between the HF radar (blue line) and the subsurface point-wise current meter (red line).

The Figure 17 indicates the quality of the data which is being used for comparisons. In this example, the red dots are the QC flag values for the current meter current speed and direction. During that period, the value was=1 (good data). For the HF radar (in blue), the QC flags are the same for both variables (i.e. speed and direction) at the nearest point to the location of the current meter. The percentage of good and probably good data is shown for each instrument in the legend. Other values (=3 probably bad and =9 missing) different from 1 or 2 are also shown for HFR data.

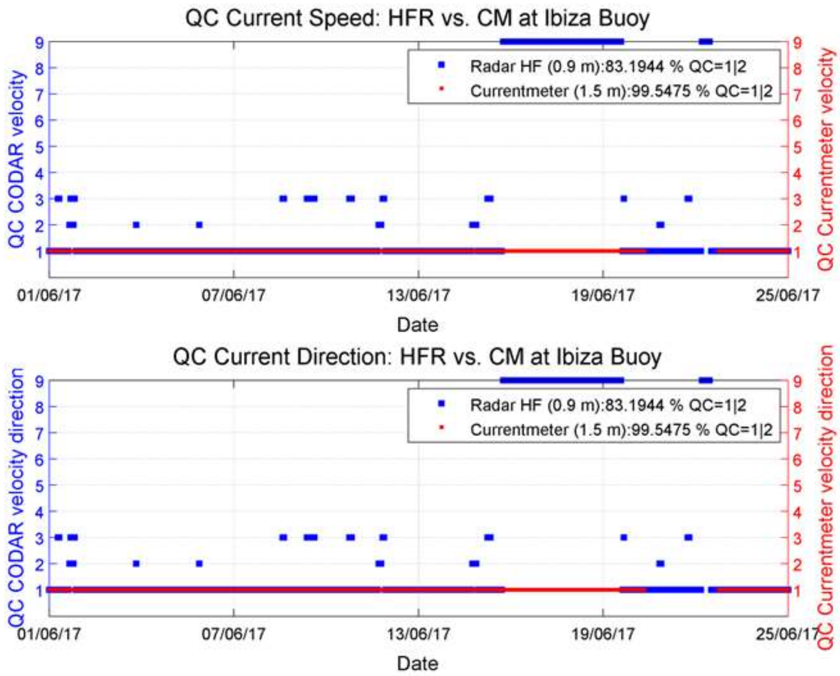

Figure 17: Time-series of QC flags values ranging from 1 to 9 (following the ARGO quality flag scale and as described in the associated PUM of the product CMEMS-INS-PUM-013_044. QC = 1 is for good data) for surface current speed (top) and current direction (bottom) for the HF radar (blue dots) and the subsurface point-wise current meter (red dots) at the nearest HFR grid point to the location of the currentmeter.

The quantile-quantile plots of Figure 18 are used to determine whether or not the distributions of the two data sets, HFR and current meter, are similar. We see here that these distributions differ only slightly near the highest values of the currents, elsewhere are very consistent.

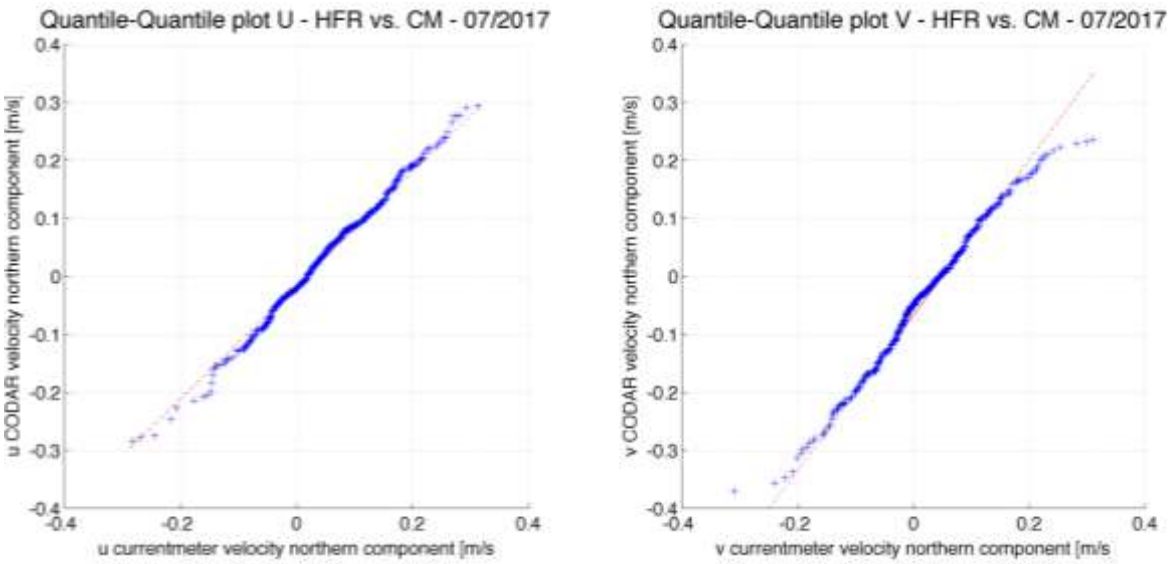

Figure 18: Quantile-quantile plots for the zonal (left) and meridional (right) surface current velocity components between the HF radar and the subsurface point-wise current meter.

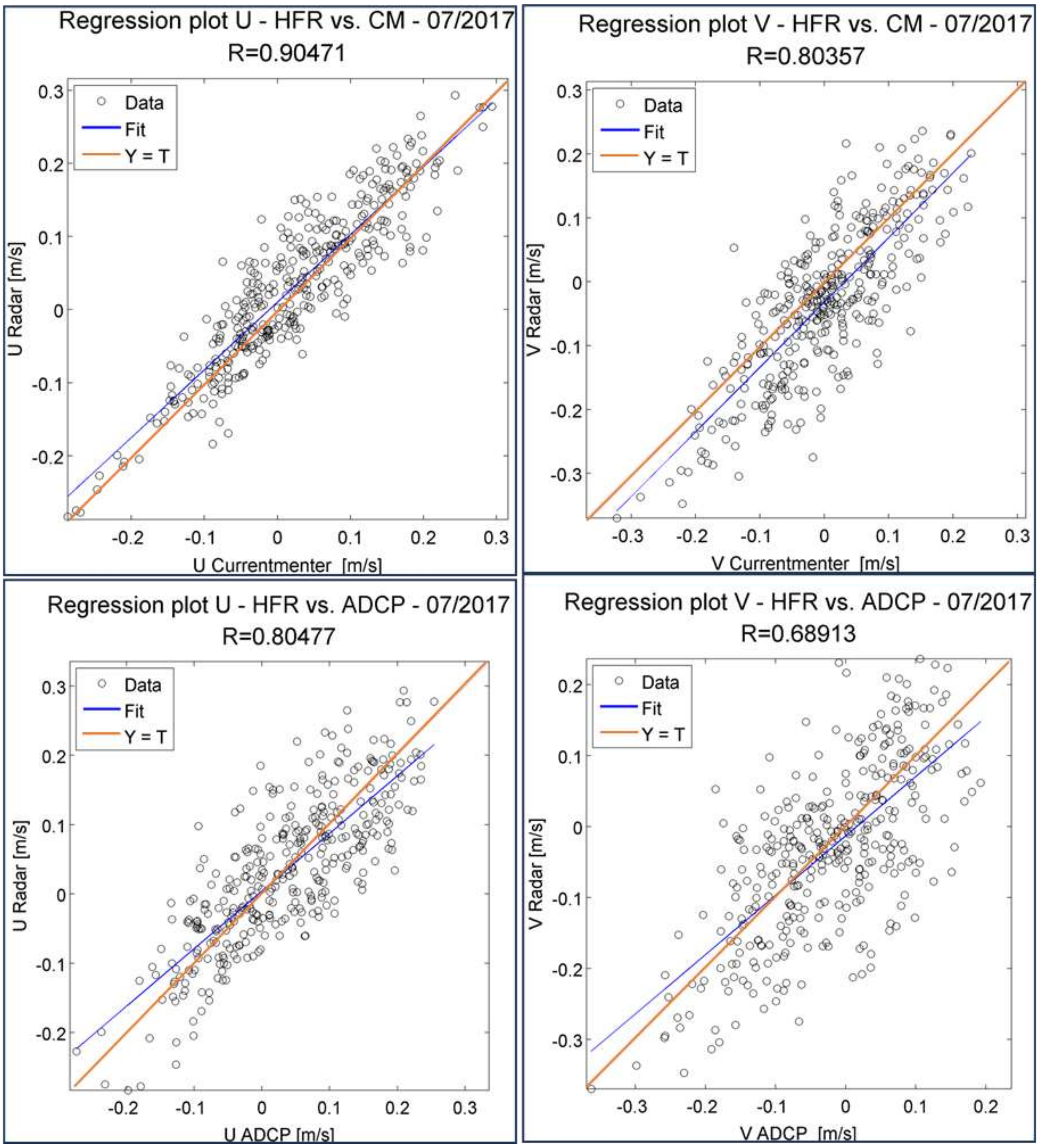

Figure 19: Regression plots for the zonal (left) and meridional (right) surface current velocity components between the HF radar and subsurface point-wise current meter (CM) -top panel- and the first bin of the Acoustic Doppler Current Profiler (ADCP) -bottom panel-.

South-eastern Bay of Biscay

Two High Frequency (HF) radar stations have been working operationally in the south-eastern part of the Bay of Biscay since 2009. They provide hourly surface currents with 5 km spatial resolution and a radial coverage close to 180 km. The QC procedures applied to HFR total velocities are a velocity threshold and a GDOP threshold. Thus, these data were not processed for all the mandatory QC tests defined by the European common QC model. The validation exercise has been done with historical data for the period 2009–2018.

Within the period 2009-2011, radar_total currents have been compared with currents at 1.5 m (data series from Donostia and Matxitxako buoys) and a drifter trajectory (Table 9). In both cases, in-situ data have been averaged using a 3-h running mean to be consistent with the processing of radar data (radar velocity data are obtained from the spectra of the received echoes every 20 minutes using the MUSIC algorithm and applying a centred 3 h running mean average). The comparison between different measuring systems is not straightforward since each system measure currents over different spatial and temporal scales and has its own inaccuracies. At 4.5 MHz frequency, the measurements made by the radar integrate currents vertically within the first 2-3 m of the water column; moreover, the radar horizontal resolution ranges geographically from several kms near the antennas, south of the domain, to several tens of kms at the middle of it. As a result, any vertical or horizontal shear in currents will contribute to the differences observed between measurements. Over the slope, better agreement is found for the east-west component at Matxitxako location, which could be linked to the less variable regime of the along-slope circulation and lower vertical shear values (for more detail see Rubio et al., 2011). The comparison with the pseudo-eulerian velocities derived from the drifter show slightly poorer agreement than in Matxitxako, which was expected as radar inaccuracies increase with the distance to the antennas.

		RMS [m·s^{-1}]				RMSD [m·s^{-1}] Data set 1 vs. data set 2		R Data set 1 vs. data set 2		MRD Data set 1 vs. data set 2	
Data set 1	Data set 2	Data set 1		Data set 2		u	v	u	v	u	v
		u	v	u	v						
Matxitxako 1.5 m	Radar	0.16	0.10	0.13	0.08	0.08	0.08	0.86	0.64	-1.10	-0.92
Matxitxako 12 m	Radar	0.15	0.09	0.13	0.08	0.10	0.09	0.74	0.50	-1.85	-2.70
Donostia 1.5 m	Radar	0.12	0.11	0.11	0.12	0.10	0.13	0.53	0.35	-1.31	0.44
Donostia 12 m	Radar	0.10	0.08	0.11	0.12	0.10	0.13	0.37	0.21	0.84	-0.22
Drifter	Radar	0.27	0.27	0.16	0.21	0.16	0.09	0.72	0.91	-0.22	-0.01
Matxitxako 1.5 m	Matxitxako 12 m	0.16	0.10	0.15	0.09	0.10	0.09	0.80	0.60	1.97	0.60
Donostia 1.5 m	Donostia 12 m	0.12	0.11	0.10	0.08	0.12	0.12	0.37	0.28	-1.36	-0.83

Table 9: Summary of comparisons between in-situ (at 1.5 and 12 m depth from moorings and at 8 m depth from the drifter) and radar-derived velocities at the corresponding nodes (Rubio et al. 2011). In order to highlight the vertical shear at each mooring location, the in-situ current measurements at 1.5 and 12 m are also compared. The Root Mean Square (RMS) for each velocity component of the compared data set is given in columns 1 to 4. The RMS deviations (RMSD), the correlation coefficient (R), and the Mean Relative Differences (MRD) between data sets, for each velocity component, are also shown in this table.

Further comparisons have been carried out using an extended drifter data set (Solabarrieta et al. 2014, 2016), consisting of pseudo-eulerian velocities computed from 20 drifter buoys launched during several campaigns within the Bay of Biscay (Charria et al., 2013). All the buoys had similar characteristics, with a surface float linked to a long (~10 m long × ~1 m wide) holey sock drogue by a thin (~5 mm) cable and centred at 15 m depth. In this case the correlation and RMSD results are poorer, as was to be expected, due to the target depth of the drifter data.

Figure 21 shows a series of Hovmöller diagrams of surface cross-transects from HFR and vertical profiles from two downward looking ADCP (see Figure 20).

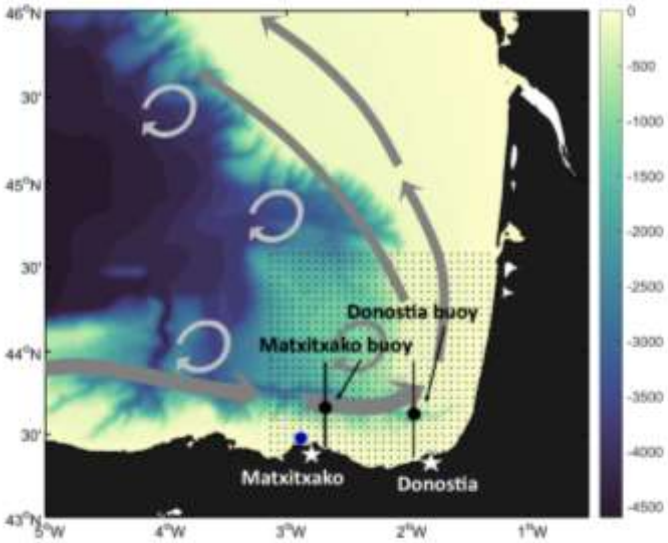

Figure 20: Study area corresponding to the south-eastern Bay of Biscay and schematic view of the winter shelf-slope current and mesoscale regime. The nodes for the computation of HF radar total currents are shown by the grey dots. The stars provide the location of the HF radar antennas in Matxitxako and Higer (Donostia) Capes. The black dots provide the location of the slope moorings Donostia (east) and Matxitxako (west) and the black lines the surface cross-transects used to plot HF radar along-slope currents in Figure 21. The blue dot provides the location of the Bimep mooring. Bathymetry is given by color bar (in meters).

For the period 2009-2018, a qualitative comparison between (surface) HF radar data and (profile) data from ADCP has been performed at two meridional sections covering the two locations of the slope moorings (16). The zonal surface currents along the continental shelf-slope derived from the HF radar along two surface cross-transects (a & c) and from profiles up to 150 m depth from downward looking ADCP data (b & d). The data corresponds to the longitude/position of the (a & b) Matxitxako and (c & d) Donostia moorings respectively (the latitude of the buoys is shown by the horizontal line in a and c). Note that b is not available from 2014-2017. This analysis shows the spatial (over the slope and vertically in the first 150 m of the water column) and temporal coherence between HFR and ADCP in the observation of seasonal and mesoscale variability.

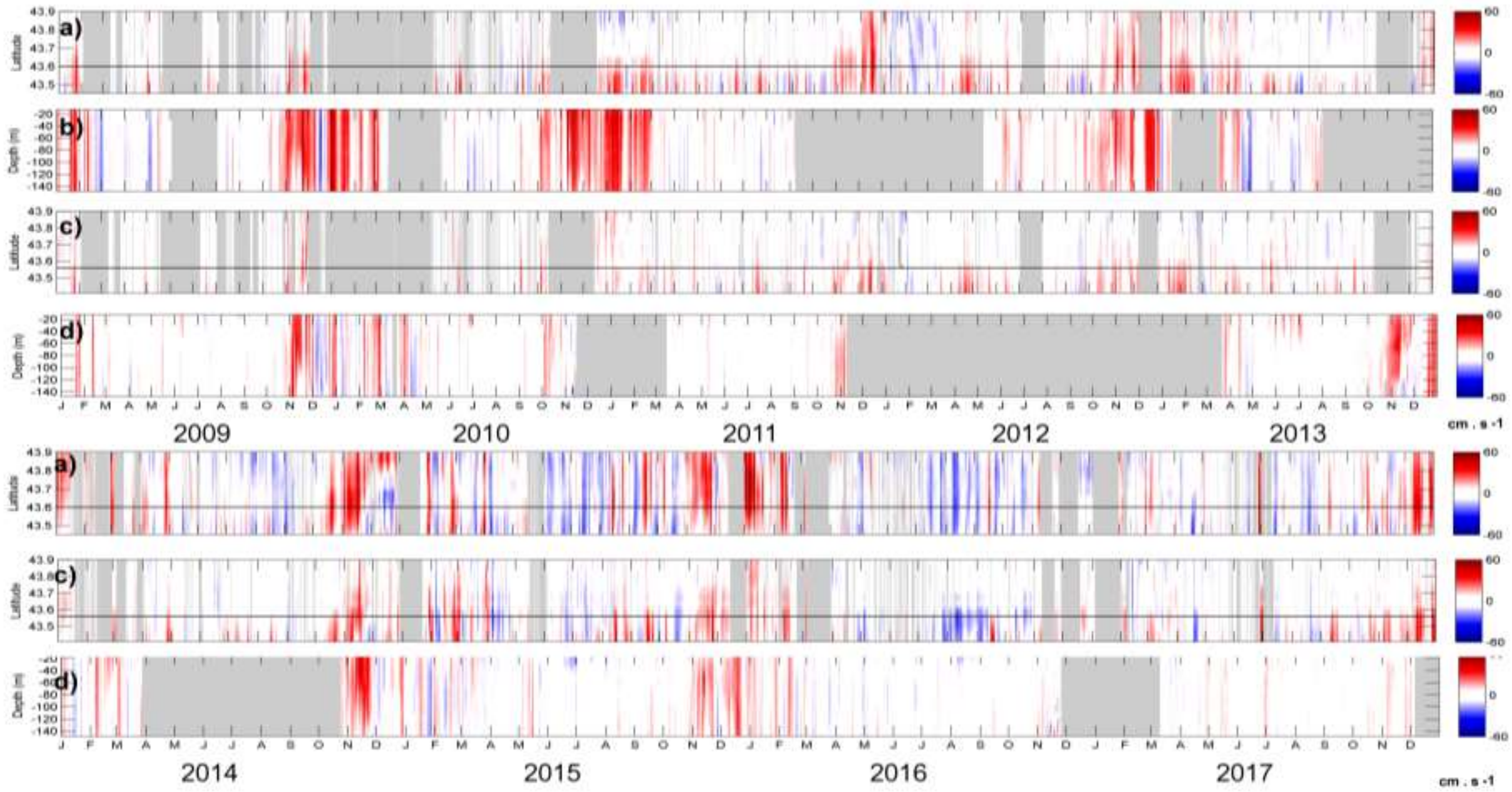

Figure 21: Hovmöller diagrams of currents along the continental shelf slope currents derived from the HFR along two surface cross-transects at the longitude of the (a) Matxitxako and (c) Donostia moorings (the latitude of the buoys is shown by the horizontal line in a and c). Hovmöller diagrams of along-slope current profiles up to 150 m depth from downward looking ADCP data in (b) Matxitxako and (d) Donostia moorings (grey shows data gaps). Note that b is not available from 2014-2017

In conclusion, the validation results for the three analysed areas show a good agreement between HFR and ADCP, drifters and current meter data in terms of total currents. With correlation ranging between 0.6 and 0.8 for most of the cases where subsurface current data from moorings or drifters within (or close to) the vertical range of the HFR measurements are used.

A specific validation exercise for radial currents was performed using low-pass filtered (T<48 h) data from the ADCPs in the Donostia and Matxitxako moorings and a third mooring (Bimep) located at 43º 28' 9.34"N 2º 53' 0.18"W for the period 2009-2011. To compare directly HFR radial currents (also low-pass filtered) with total currents from the ADCPs, the ADCP currents were projected into the radial directions covered by each of the EuskOOS HF radar stations (Higher and Matxitxako) with contained measurement points closest to the location of the corresponding mooring. The comparison was done in terms of Pearson’s correlation. The correlation between the temporal series of ADCP currents and the HFR radial currents from the two antennas are shown in Table 10.

Mooring (depth of the measurement)	HFR site	R
MATX (12 m)	MATX	0.60
	HIGE	0.54
DONOSTIA (12 m)	MATX	0.24
	HIGE	0.48
BIMEP (11 m)	MATX	0.90
	HIGE	0.77

Table 10: Correlation between the temporal series of ADCP currents in three different moorings and the HFR radial currents from the two antennas.

As in the case of total currents, the analysis of the results in the comparison between different measuring systems is not straightforward since each system measure currents over different spatial and temporal scales, and any vertical (the ADCP data used for comparison is between 11 and 12 m depth) or horizontal shear in currents will contribute to the differences observed. The best agreement is found for the comparisons in the Bimep mooring, with correlations up to R=0.9 with the radial data from Matxitxako antenna. Again, a better agreement is found on the continental slope for the radial direction that are more influenced by the east-west component of the slope-current.

Another recent exercise was performed in Manso-Narvarte et al. (2018), where HFR radial currents were compared to altimetry data following the approach previously applied in Liu et al. (2012). It consisted in the direct comparison between HFR and altimetry data in a certain point, where one of the HFR radial directions crosses the altimeter track perpendicularly. This approximation allowed to directly use the radar radial currents, which are in the same direction than the across-track geostrophic currents. The results provide an evaluation of the performance of both datasets (altimetry and HFR) within the study area and a better understanding of the ocean variability contained in the corresponding measurements. Again, the highest correlations (up to 0.64) where observed over the slope.

IV.3 Argo dataset

For the “argo” dataset, the KPIs are available on http://www.marineinsitu.eu/monitoring/
The KPIs major indicators for Argo dataset are:

- Timeliness of delivery
- Number of platforms operating per day
- Data quality flag percentages during specified period in months

- Parameter availability

The dataset is regularly validated by a specialist from Ifremer with:

- A global interactive current speed map (Figure 5 and Figure 22)
- Graphs and maps of current speed per float (Figure 25 and Figure 26)

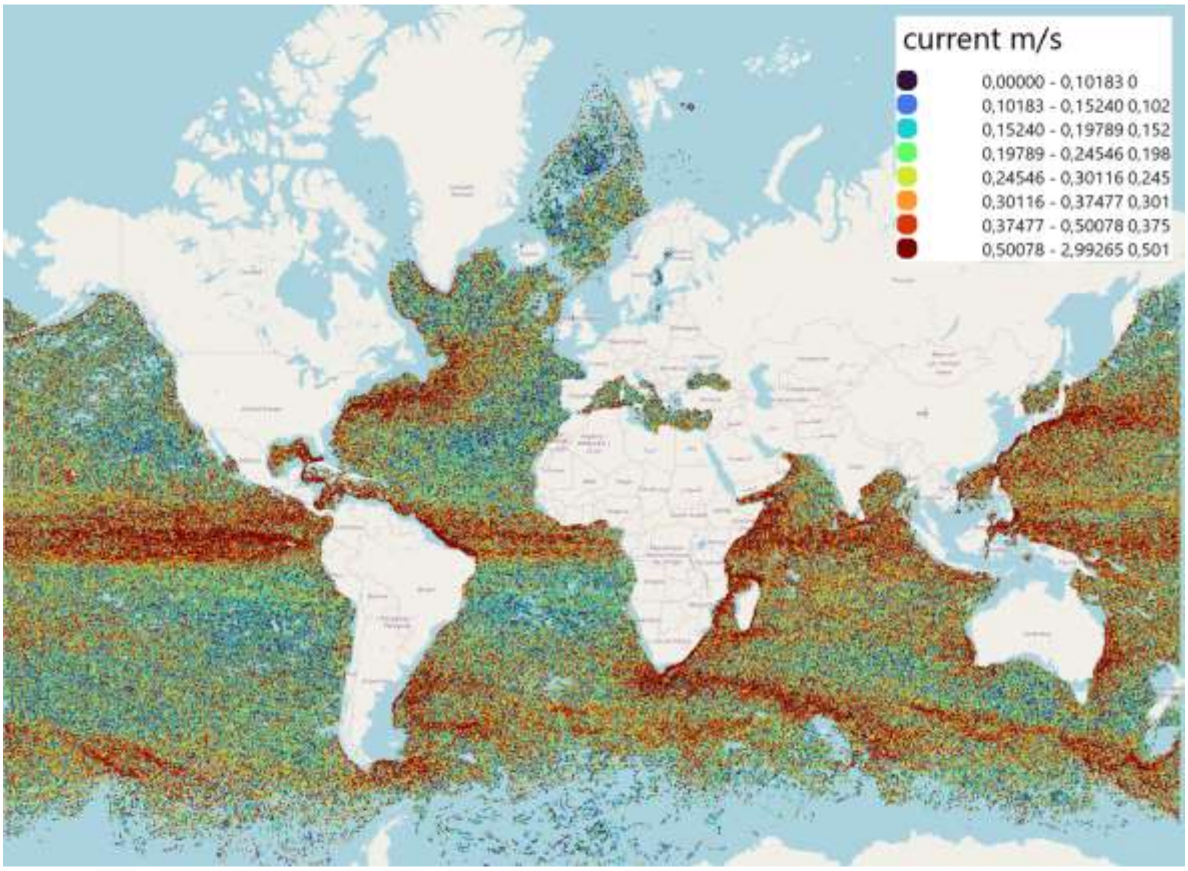

Figure 22: *Map of Argo surface ocean currents. Each dot represents the surface current from one cycle (typically a few hours in surface) from one float.*

The Figure 23 and Figure 24 give an overview of the distribution of the velocities and the pressure values of the deep ocean currents. The depth of deep Argo drift is around 1000 meter for the vast majority of the floats.

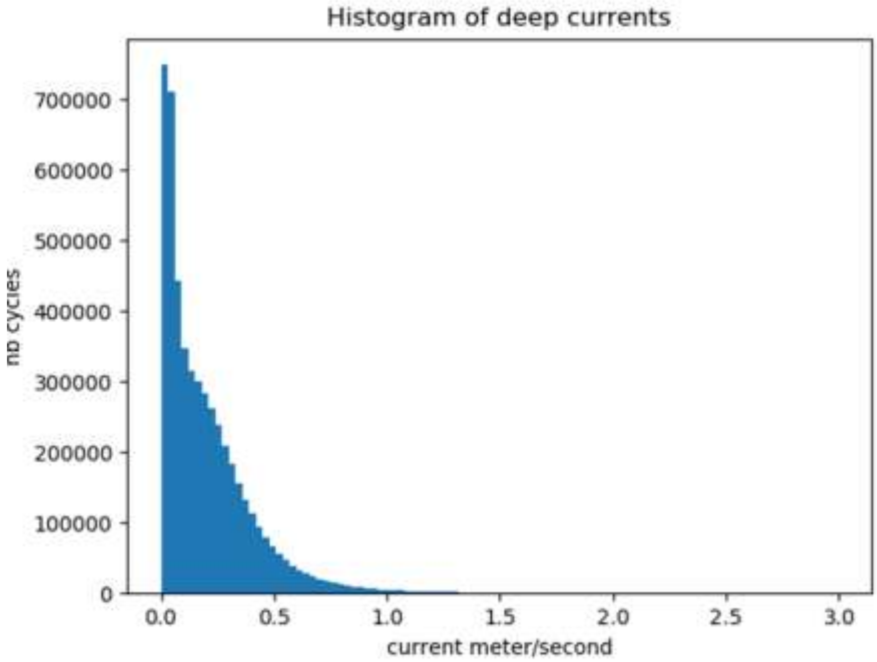

Figure 23: ***Distribution of Argo deep ocean current (one cycle : 10 days deep water drift of an Argo float provides one deep current observation).***

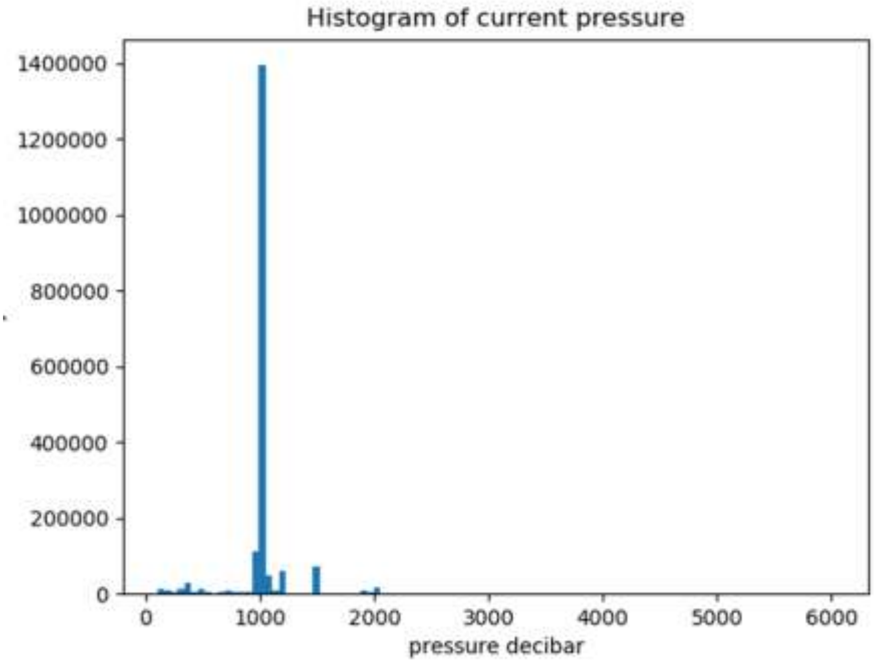

Figure 24: ***The vast majority of Argo floats have a 10 days deep water drift at 1000 decibars (around 1000 meter deep).*** *A very small number of trajectories, therefore not visible on the figure, are around 6000 decibars.*

On April 2023, the Argo current dataset had 5 million records of current with values from 0 to 2.1496 meters/second (Table 11).

Statistic Name	value
Minimum current m/s	0.0000
Maximum current m/s	2.1496
Median current m/s	0.0393
Mean current m/s	0.550
Number of cycles	5 065 172

Table 11: Argo deep currents statistics

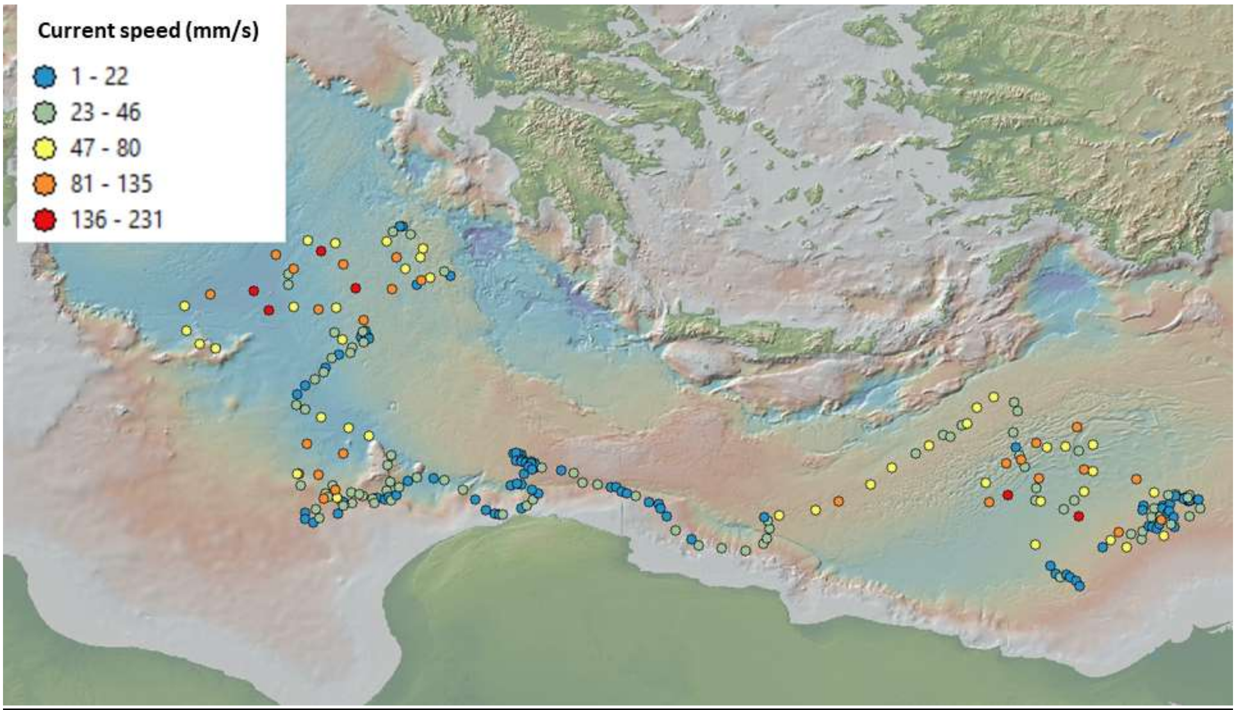

Figure 25: Argo current from float 6900967 in the Mediterranean Sea and around 350m depth: Colors indicate current speed from 1 mm/s to 231 mm/s.

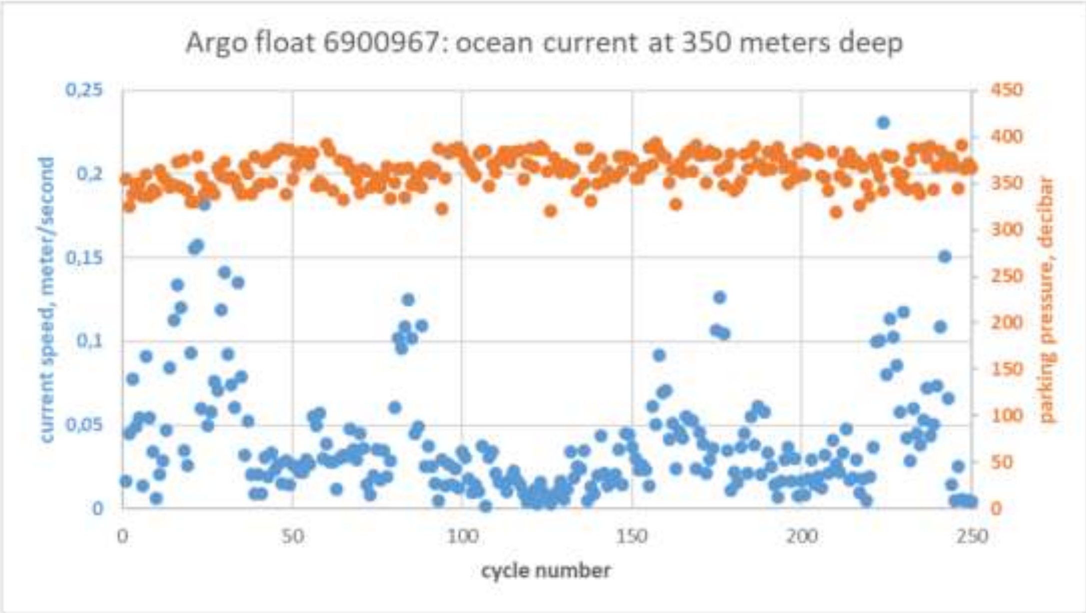

Figure 26: Argo current from float 6900967 (same as in Figure 25) around 350 meter deep.

V SYSTEM'S NOTICEABLE EVENTS, OUTAGES OR CHANGES

Date	**Change/Event description**
16/04/2019	Creation of the product
December 2020	Addition of Argo currents dataset (cmems_obs-ins_glo_phy-cur_nrt_argo_irr))
November 2022	Drifter_filt dataset removal, new data for Mediterranean region (MO_TS_DC files)
November 2023	Since November 2022, some US drifters data are not available anymore due to the high cost of the Iridium transmission. This represents around 250 drifters.
November 2023	Addition of undrogued drifter data, additional Argo deep currents from AOML (Pacific Ocean mainly)

VI QUALITY CHANGES SINCE PREVIOUS VERSION

Since the update of the product in November 2022, additional dataset with file nomenclature MO_TS_DC (Mediterranean data), are added in the NRT UV product inside the cmems_obs-ins_glo_phy-cur_nrt_drifter_irr dataset.

Since the update of the product in November 2023, data from drifters that have lost their drogue are now disseminated. The coverage of deep velocities from Argo Floats has also been improved, in particular in the Pacific Ocean.

VII REFERENCES

Barrick, D.E., Evans M.W, Weber B.L (1977) Ocean surface currents mapped by radar. Science, 198 (Available at http://www.codar.com/images/about/1977Barrick_Science.pdf)

Barrick, D. (2002). Geometrical dilution of statistical accuracy (GDOSA) in multi-static HF radar networks. Codar ocean sensors, (Available at http://www. codaros. com/Manuals/SeaSonde/Docs/Informative/GDOSA Definition. pdf).

Chapman, R.D., Shay, L., Graber, H., Edson, J., Karachintsev, A., Trump, C., Ross, D. (1997). On the accuracy of HF radar surface current measurements: Intercomparisons with ship-based sensors. J. Geophys. Res.-Oceans (1978–2012),102, C8, 18 737–18 748

Charria, G., Lazure, P., Le Cann, B., Serpette, A., Reverdin, G., Louazel, S., Batifoulier, F., Dumas, F., Pichon, A., Morel, Y., 2013. Surface layer circulation derived from Lagrangian drifters in the Bay of Biscay. J. Mar. Syst. 109–110, S060–076 http://dx.doi.org/10.1016/j.jmarsys.2011.09.015

Corgnati et al, 2018 Building strong foundations towards a pan-European High Frequency Radar network. https://imdis.seadatanet.org/content/download/122304/file/S3P104_IMDIS2018.pdf

Corgnati L., Mantovani C., Griffa A., Berta M., Penna P., Celentano P., Bellomo L., Carlson D.F., and D'Adamo R., 2018, "Implementation and Validation of the ISMAR High-Frequency Coastal Radar Network in the Gulf of Manfredonia (Mediterranean Sea)," in IEEE Journal of Oceanic Engineering. doi: 10.1109/JOE.2018.2822518.

Elipot S., Lumpkin R., Perez R.C., Lilly J.M., Early J.J, Sykulsi A.M. (2016). A global surface drifter data set at hourly resolution. JGR, 121 (5), p2937-2966., https://doi.org/10.1002/2016JC011716.

EuroGOOS DATA-MEQ working group (2010). Recommendations for in-situ data Near Real Time Quality Control. https://doi.org/10.13155/36230

Gurgel, K.W., Essen, H.H., Kingsley, S. (2019) HF radars: Physical limitations and recent developments.

Hansen, D. V., and P.-M. Poulain (1996), Quality control and interpolationsof WOCE-TOGA drifter data,J. Atmos. Oceanic Technol.,13, 900–909.

Herbert Gaelle (2020). Qualification temps réel des données trajectoire des flotteurs Argo. https://doi.org/10.13155/95169

Kalampokis, A., Uttieri, M., Poulain, P. M., Zambianchi, E. (2016). Validation of HF Radar-Derived Currents in the Gulf of Naples With Lagrangian Data. IEEE Geosci. Remote Sens. Lett., doi: 10.1109/LGRS.2016.2591258

Kohut, J. T. and Glenn, S. M. (2003). Improving HF radar surface current measurements with measured antenna beam patterns. J. Atmos. Ocean. Tech., 20, 1303–1316, 2003.

Lana, A., Fernández, V., Tintoré, J. (2015) SOCIB Continuous Observations Of Ibiza Channel Using HF Radar. Sea Technology 56, 31-34.

Lana, A., Marmain, J., Fernández, V., Tintoré, J., Orfila, A. (2016) Wind influence on surface current variability in the Ibiza Channel from HF Radar. Ocean Dynamics 66, 483-497.

Lipa, B. 2013. Uncertainties in SeaSonde current velocities. Proc. of the IEEE/OES Seventh Working Conference on Current Measurement Technology. DOI: 10.1109/CCM.2003.1194291 · Source: IEEE Xplore

Liu, Y., Weisberg, R. Merz, C., Lichtenwalner, S., and Kirkpatrick, G. (2010). HF radar performance in a low-energy environment: Codar Seasonde experience on the west Florida shelf. J.Atmos.OceanicTechnol. 27,1689–1710. doi:10.1175/2010JTECHO720.1

Liu, Y., Weisberg, R. H., Vignudelli, S., Roblou, L., and Merz, C. R.: Comparison of the X-TRACK altimetry estimated currents with moored ADCP and HF radar observations on the West Florida Shelf, Adv. Space Res., 50, 1085–1098, https://doi.org/10.1016/j.asr.2011.09.012, 2012.

Lorente, P., Aguiar, E., Bendoni, M., Berta, M., Brandini, C., Cáceres-Euse, A., Capodici, F., Cianelli, D., Ciraolo, G., Corgnati, L., Dadić, V., Doronzo, B., Drago, A., Dumas, D., Falco, P., Fattorini, M., Gauci, A., Gómez, R., Griffa, A., Guérin, C.-A., Hernández-Carrasco, I., Hernández-Lasheras, J., Ličer, M., Magaldi, M. G., Mantovani, C., Mihanović, H., Molcard, A., Mourre, B., Orfila, A., Révelard, A., Reyes, E., Sánchez, J., Saviano, S., Sciascia, R., Taddei, S., Tintoré, J., Toledo, Y., Ursella, L., Uttieri, M., Vilibić, I., Zambianchi, E. and Cardin, V.: Coastal high-frequency radars in the Mediterranean -- Part 1: Status of operations and a framework for future development, Ocean Sci., 18(3), 761–795, doi:10.5194/os-18-761-2022, 2022.

Mader, J., Rubio, A., Asensio, J.L., Novellino, A., Alba, M., Corgnati, L., et al. THE EUROPEAN HF RADAR INVENTORY(2017) http://eurogoos.eu/download/reference_documents_/EU_HFRadar_inventory.pdf

Manso-Narvarte, I., Caballero, A., Rubio, A., Dufau, C, Birol, F (2018). Joint analysis of coastal altimetry and high-frequency radar data: observability of seasonal and mesoscale ocean dynamics in the Bay of Biscay. Ocean Sci. doi:10.5194/os-2018-33.

Menna M, Gerin R, Bussani A, Poulain P-M (2017). The OGS Mediterranean drifter dataset: 1986-2016.OGS 2017/92 OCE 28 MAOS. 34pp. http://maos.inogs.it/pub/Menna%20et%20al%202017_Drifter_database.pdf

Menna M, Poulain P-M, Bussani A, Gerin R. (2018). Detecting the drogue presence of SVP drifters from wind slippage in the Mediterranean Sea. . Measurement, 125, 447-453. https://doi.org/10.1016/j.measurement.2018.05.022.

Molcard, A., Poulain, P. M., Forget, P., Griffa, A., Barbin, Y., Gaggelli, J., De Maistre, J. C., Rixen, M. (2009). Comparison between VHF radar observations and data from drifter clusters in the Gulf of La Spezia (Mediterranean Sea), J. Mar. Sys., 78S, S79-S89.

Ohlmann C., White, P., Washburn, L., Emery, B., Terrill, E., Otero, M. (2007). Interpretation of Coastal HF Radar–Derived Surface Currents with High-Resolution Drifter Data. J. Atmos. Oceanic Technol, 24(4), 666-680.

Ollitraut M. and J-P Rannou (2013). ANDRO: An Argo-based deep displacement dataset. JAOTech, 759-788. DOI:10.1175/JTECH-D-12-00073.1

Ollitrault Michel, Rannou Jean-Philippe (2013). ANDRO Dataset contents and format. https://archimer.ifremer.fr/doc/00360/47126

Paduan, J.D., Rosenfeld, L.K. (1996) Remotely sensed surface currents in Monterey Bay from shore-based HF radar (Coastal Ocean Dynamics Application Radar). Journal of Geophysical Research: Oceans 101, 20669-20686

Paduan, J.D., Graber, H.C. (1997) Introduction to high-frequency radar: Reality and myth. Oceanography 10, 4.

Poulain P.M, M. Menna, E. Mauri (2012). Surface geostrophic circulation of the Mediterranean Sea derived from drifters and satellite altimeter data. JPO, 42 (6). doi:10.1175/JPO-D-11-0159.1)

Révelard, A., Reyes, E., Mourre, B., Hernández-Carrasco, I., Rubio, A., Lorente, P., Fernández, C. D. L., Mader, J., Álvarez Fanjul, E., and Tintoré, J.: Sensitivity of Skill Score Metric to Validate Lagrangian Simulations in Coastal Areas: Recommendations for Search and Rescue Applications, Frontiers in Marine Science, 8, https://www.frontiersin.org/articles/10.3389/fmars.2021.630388, 2021

Reyes, E., Aguiar, E., Bendoni, M., Berta, M., Brandini, C., Cáceres-Euse, A., Capodici, F., Cardin, V., Cianelli, D., Ciraolo, G., Corgnati, L., Dadić, V., Doronzo, B., Drago, A., Dumas, D., Falco, P., Fattorini, M., Fernandes, M. J., Gauci, A., Gómez, R., Griffa, A., Guérin, C.-A., Hernández-Carrasco, I., Hernández-Lasheras, J., Ličer, M., Lorente, P., Magaldi, M. G., Mantovani, C., Mihanović, H., Molcard, A., Mourre, B., Révelard, A., Reyes-Suárez, C., Saviano, S., Sciascia, R., Taddei, S., Tintoré, J., Toledo, Y., Uttieri, M., Vilibić, I., Zambianchi, E. and Orfila, A.: Coastal high-frequency radars in the Mediterranean -- Part 2: Applications in support of science priorities and societal needs, Ocean Sci., 18(3), 797–837, doi:10.5194/os-18-797-2022, 2022.

Roarty, H., Smith, M., Kerfoot, J., Kohut, J. and Glenn, S. (2012). Automated quality control of High Frequency radar data. *2012 Oceans*, Hampton Roads, VA, pp. 1-7. doi: 10.1109/OCEANS.2012.6404809

Rubio A, Reverdin G, Fontán, A., González, M., Mader, J., 2011. Mapping near-inertial variability in the SE Bay of Biscay from HF radar data and two offshore moored buoys. Geophys. Res. Lett., 38 (19): L19607.

Rubio A, Mader J, Corgnati L, Mantovani C, Griffa A, Novellino A, Quentin C, Wyatt L, Schulz-Stellenfleth J, Horstmann J, Lorente P, Zambianchi E, Hartnett M, Fernandes C, Zervakis V, Gorringe P, Melet A and Puillat I (2017). HF Radar Activity in European Coastal Seas: Next Steps Towards a Pan-European HF Radar Network. Front. Mar. Sci. 4:8. doi: 10.3389/fmars.2017.00008

Rubio et al. 2018. Present and future of the European HF radar network: outcomes of the INCREASE project. Proceedings of the 4th Orca meeting. Okinawa (Japan). http://orca2018.official.jp/wp-content/uploads/2018/05/ExtendedAbstract_Session4.pdf

Sentchev A., Forget P., and Faunié P., “Surface current dynamics undersea breeze conditions observed by simultaneous HF radar, ADCP and drifter measurements,” Ocean Dyn., vol. 67, no. 3–4, pp. 499–512, 2017.

Solabarrieta, L., Frolov, S., Cook, M., Paduan,J., Rubio, A., González,M., Mader, J., Charria, G., 2016. Skill assessment of HF radar-derived products for lagrangian simulations in the Bay of Biscay. J. Atmos. Oceanic Technol., in press, doi: 10.1175/JTECH-D-16-0045.1.

Solabarrieta, L., Rubio, A., Castanedo, S., Medina, R., Fontán, A., González, M., Fernández, V., Charria, G., Hernández, C., 2014. Surface water circulation patterns in the southeastern Bay of Biscay: New evidences from HF radar data. Cont. Shelf. Res., 74: 60-76.

Argo (2020). Argo float data and metadata from Global Data Assembly Centre (Argo GDAC). SEANOE. https://doi.org/10.17882/42182